frontiers | Frontiers in Earth Science

ORIGINAL RESEARCH
published: 05 July 2022
doi: 10.3389/feart.2022.868357

Tree-Ring Isotopic Records Suggest Seasonal Importance of Moisture Dynamics Over Glacial Valleys of the Central Himalaya

*Nilendu Singh[1,2], Mayank Shekhar[3], Bikash Ranjan Parida[4], Anil K. Gupta[5], Kalachand Sain[2], Santosh K. Rai[2], Achim Bräuning[6], Joyeeta Singh Charkaborty[7], Vikram Sharma[8], Reet Kamal Tiwari[9], Pankaj Chauhan[2] and Leonardo Montagnani[1]**

[1]Tree Ecophysiology and Ecosystem Research Unit, University of Bolzano, Bolzano, Italy, [2]Wadia Institute of Himalayan Geology, Dehradun, India, [3]Birbal Sahni Institute of Palaeosciences, Lucknow, India, [4]Department of Geoinformatics, School of Natural Resource Management, Central University of Jharkhand, Ranchi, India, [5]Department of Geology and Geophysics, Indian Institute of Technology Kharagpur, Kharagpur, India, [6]Institute of Geography, University of Erlangen–Nuremberg, Erlangen, Germany, [7]Forest Research Institute, Dehradun, India, [8]Department of Geography, Institute of Science, Banaras Hindu University, Varanasi, India, [9]Department of Civil Engineering, Indian Institute of Technology Ropar, Ropar, India

OPEN ACCESS

Edited by:
Moritz Felix Lehmann,
University of Basel, Switzerland

Reviewed by:
William Anderson,
Florida International University, United States
Feng Chen,
Yunnan University, China
Rolf Siegwolf,
Swiss Federal Institute for Forest, Snow and Landscape Research (WSL), Switzerland

***Correspondence:**
Leonardo Montagnani
leonardo.montagnani@unibz.it

Specialty section:
This article was submitted to Biogeoscience, a section of the journal Frontiers in Earth Science

Received: 02 February 2022
Accepted: 06 June 2022
Published: 05 July 2022

Citation:
Singh N, Shekhar M, Parida BR, Gupta AK, Sain K, Rai SK, Bräuning A, Singh Charkaborty J, Sharma V, Kamal Tiwari R, Chauhan P and Montagnani L (2022) Tree-Ring Isotopic Records Suggest Seasonal Importance of Moisture Dynamics Over Glacial Valleys of the Central Himalaya. Front. Earth Sci. 10:868357. doi: 10.3389/feart.2022.868357

Accelerated glacier mass loss is primarily attributed to greenhouse-induced global warming. Land–climate interactions have increasingly been recognized as an important forcing at the regional-local scale, but the related effects on the Himalayan glaciers are less explored and thought to be an important factor regulating spatial heterogeneity. The aim of the present study is a multi-decadal approximation of glacier—hydroclimate interaction over the western region of the central Himalaya (WCH). Multi-species, highly coherent, tree-ring cellulose $\delta^{18}O$ chronologies from three sites across the WCH were used to derive atmospheric humidity (Atmospheric Moisture Content: AMC) record of the last four centuries. Annual-scale AMC reconstruction implies a decreasing regional atmospheric moisture since the mid-19th century and a sharp decline in recent decades (1960s). Coherency analyses between regional AMC and glacier mass balance (GMB) indicate an abrupt phase-shift in the relationship after the 1960s within a common record of the last 273 years. To ascertain the cause of this phase-shift, annual AMC was disintegrated into seasonal-scale, utilizing ~200 years of $\delta^{18}O$ record of a deciduous tree species. Seasonal (winter: October–March; summer: April–September) AMC reconstructions and disaggregation results indicate higher sensitivity of regional ice-mass variability to winter moisture dynamics than summer.Winter season AMC reconstruction confirms a revival of winter westerlies-driven moisture influx in the region since the 1970 s. Meanwhile, the record for the summer season AMC indicates a gradual decline in moisture influx from the beginning of the 20th century. Interestingly, despite a prominent decline in Indian summer monsoon (ISM) precipitation after the mid-20th century, the summer season AMC—GMB relation remained stable. We hypothesize that decadal-scale greening, and consequently increased evapotranspiration and pre-monsoon precipitation might have been recycled through the summer season, to compensate for the ISM part of precipitation. However, isotope-enabled ecophysiological models and measurements would strengthen this hypothesis. In addition, high-resolution radiative forcing and

long-term vegetation greening trends point towards a probable influence of valley greening on GMB. Our results indicate that attribution of ice mass to large-scale dynamics is likely to be modulated by local vegetation changes. This study contributes to the understanding of long-term hydroclimate—ice mass variability in the central Himalaya, where predictions are crucial for managing water resources and ecosystems.

Keywords: glacier-climate interactions, tree-ring isotopes, greening, westerly, ISM, central himalayan glaciers

1 INTRODUCTION

Glaciers of the Himalaya–Karakoram–Tibetan Plateau (HKT) orogeny sustain water resource for downstream countries and also form a region of complex hydroclimatic patterns (Fujita and Nuimura, 2011; Yao et al., 2012; Kapnick et al., 2014; Misra et al., 2015; Sakai and Fujita, 2017; Bonekamp et al., 2019; Yao et al., 2019; Wang et al., 2019; Wang et al., 2020; Chen et al., 2021). Primarily, the retreat and mass loss of these glaciers has been attributed to greenhouse warming. However, several recent studies show that local-regional forcing and feedback processes also play an important role over the glacial valleys (Lau et al., 2010; Pepin et al., 2015; de Kok et al., 2018; Yao et al., 2019; de Kok et al., 2020; Managave et al., 2020; Rashid et al., 2020; Sigdel et al., 2020). Studies also suggest that spatial heterogeneity in the HKT is locally regulated by mechanisms associated with elevation-dependent warming, regional land–climate interaction, and long-term variability in atmospheric circulation (Lau et al., 2010; Mölg et al., 2012a; Mölg et al., 2012b; Kapncik et al., 2014; Mölg et al., 2014; Pepin et al., 2015; Mölg et al., 2017; Yao et al., 2019; Managave et al., 2020; Singh et al., 2020; Singh et al., 2021a).

The climate heterogeneity in the Himalaya is even more pronounced; while many glaciers in the Karakoram appear to be stable or advancing, the glaciers in the central Himalaya exhibit considerable retreat rates (Bonekamp et al., 2019). The Himalayan glaciers are regulated by inter-decadal variability in winter-westerlies and the Indian summer monsoon (ISM) (Bookhagen and Burbank, 2010; Yao et al., 2019; Perry et al., 2020; Singh et al., 2021a). However, recent studies on differential rates of heating and elevation-dependent warming have highlighted the importance of all possible local-regional land–climate interaction and feedback processes, including vegetation-induced moisture recycling, that are capable of influencing ice-mass variability (Lau et al., 2010; Mölg et al., 2012b; Collier et al., 2013; Pepin et al., 2015; de Kok et al., 2018; Yadav et al., 2019; Yao et al., 2019; de Kok et al., 2020; Rashid et al., 2020; Sigdel et al., 2020).

Satellite datasets (e.g., GPM, TRMM) and modelling efforts (e.g., High Asia Refined Analysis, APHRODITE) have been used to analyse climate heterogeneity, however, these data-model integrations cannot be extended beyond a few decades and are too coarse to resolve regional-local changes (Yao et al., 2019; Molden et al., 2022). Further, inadequate understanding of regional land–climate interaction causes discrepancies among the projections of different climate models (Watanabe et al., 2019; Jury et al., 2020). To improve coupled glacier-climate models, it is necessary to focus on important synthetic properties of local land–climate interaction that are understood in detail at a certain scale and could be extended to larger spatial and temporal scales without loss of information.

Tree-ring stable isotopes ($\delta^{18}O$ and $\delta^{13}C$), in particular $\delta^{18}O$, provide a reliable source of multi-decadal scale hydroclimate variability due to their inherent sensitivity to climate, coherence in climatic response, and because the environmental controls regulating tree physiology are well understood (Haupt et al., 2011; Sano et al., 2012; Sano et al., 2013; Baker et al., 2016; Sano et al., 2017; Xu et al., 2017; Zeng et al., 2017; Xu et al., 2018; Huang et al., 2019; Singh et al., 2019; Singh et al., 2021a). A major part of the tree ring $\delta^{18}O$ signal should reflect variation in $\delta^{18}O$ of precipitation or atmospheric humidity, as tree roots take up soil water without fractionation of the heavier $H_2{}^{18}O$ (Baker et al., 2016; Managave et al., 2020; Lehmann et al., 2018; Lehmann et al., 2020). The mechanisms associated with the physical fractionation of stable oxygen isotopes over lower latitudes indicate that tree-ring $\delta^{18}O$ values are mainly regulated by $\delta^{18}O$ of atmospheric humidity that is driven by Rayleigh distillation. Here, we investigated three centuries of glacier—hydroclimate interaction over the western transition region in the central Himalaya (WCH) (**Figure 1**). Three coherent tree-ring cellulose $\delta^{18}O$ values are mainly regulated by $\delta^{18}O$ of atmospheric humidity (Lehmann et al., 2018; Lehmann et al., 2020), the bidirectional diffusion of water molecules between the atmosphere and sub-stomatal cavities of the leaves, which are dominated by Rayleigh distillation via amount effect, encompassing the last four centuries were used to derive regional changes in annual and seasonal (winter and summer accumulation season) atmospheric moisture content (AMC). This study utilized three centuries of glacier mass balance (GMB) data series derived from tree-ring cellulose $\delta^{13}C$ chronologies of different species growing in WCH glacial valleys, with the basic premise that climate (temperature) is a bridge that indirectly connects the mass balance of a glacier with tree-ring C isotope ratios (Singh et al., 2021a). Besides temperature, water relations (atmospheric humidity (RH) and/or soil water availability) could affect C isotope ratios. An increase in RH will result in an increase in stomatal conductance (gs), causing a decrease in the intercellular to atmospheric CO_2 (ci/ca) ratio, resulting in the lowering of $\delta^{13}C$. In contrast, a decrease in RH (dry conditions) will have an opposite effect on gs, the ci/ca ratio and $\delta^{13}C$. Moreover, the light regime (irradiation) affects the photosynthetic rate, which influences ci/ca ratio, and $\delta^{13}C$. Thus, $\delta^{13}C$ can serve as an indirect proxy for the changes in GMB. To assess long-term greening-mediated changes in local radiative

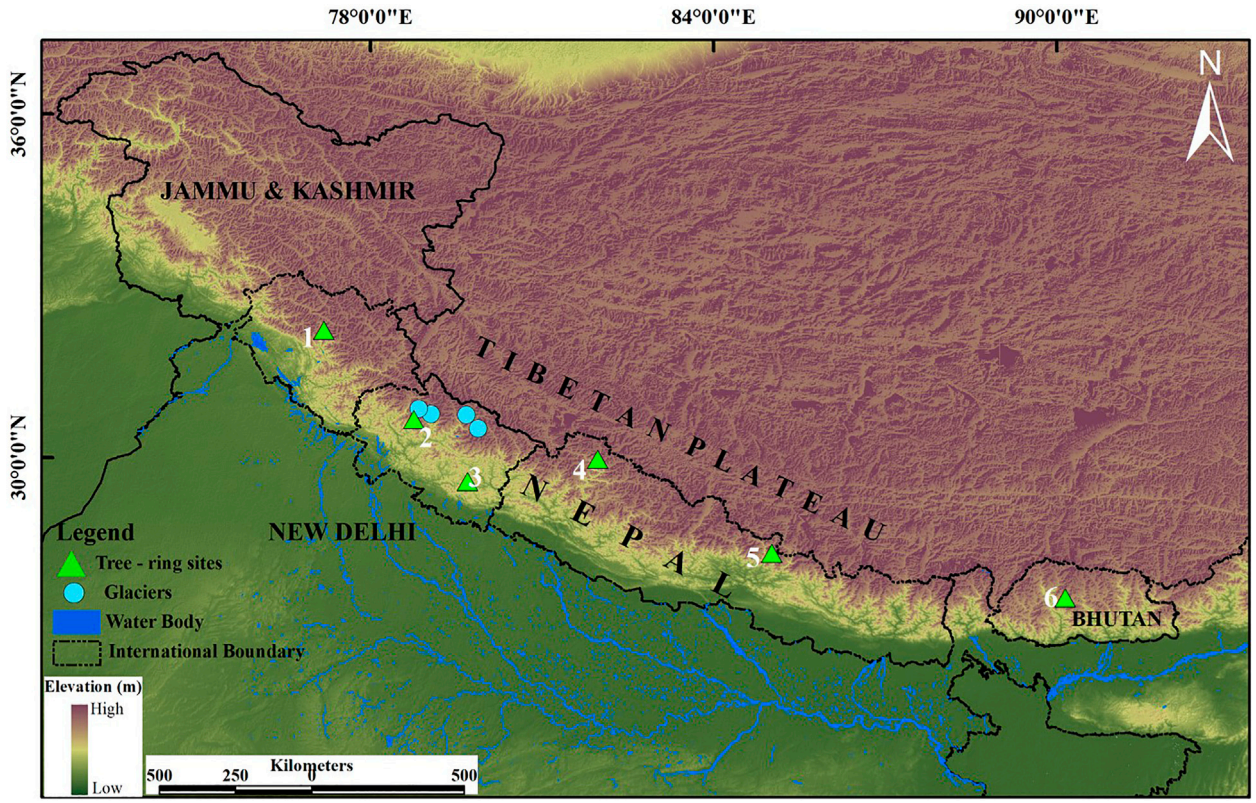

FIGURE 1 | Study region showing the location of four benchmark glaciers (Blue circles: Dokriani, Chorabari, Tipra Bamak and Dunagiri Glaciers) in the western transitional region in the central Himalaya (WCH). Green triangles (1–3) indicate the location of tree-ring sites in WCH and rest (4–6) across the central Himalaya: 1) Manali (Sano et al., 2017), 2) Uttarakashi (Singh et al., 2019), 3) Jageshwar (Xu et al., 2018), 4) Humla (Sano et al., 2012), 5) Ganesh (Xu et al., 2018), and 6) Bhutan (Sano et al., 2013).

balance, information about decadal-scale vegetation greening trends, changes in valley-scale seasonal vegetation patterns, biophysical aspects, and radiative fluxes were accessed using high-resolution satellite and CERES (Cloud and Earth Radiation Energy System) datasets. This study aims to reconstruct the annual and seasonal changes in AMC based on regional tree-ring $\delta^{18}O$ chronologies and to determine its temporal coherence with GMB with reference to the local forcing factors.

2 MATERIALS AND METHODS

2.1 Study Region and Climate

The western transition region in the central Himalaya constitutes the study region (WCH: 29° 38′–32° 13′ N and 77° 13′–80° 50′ E) (**Figure 1**). During summer, glaciers in the region are known to be fed by the Indian summer monsoon (ISM). In contrast, winter snow accumulation is influenced by a precipitation regime driven by mid-latitude winter westerlies. Long-term meteorological records of higher elevation are not readily available. Analyses of gridded Climate Research Unit (CRU) records indicate that annual regional precipitation is ~800 mm, of which the warm-wet summer months (April-September) receive about 80%. The mean annual temperature varies around 5.5°C, with a minimum (−9.4°C) in January and a maximum (~18.5°C) in July (Harris et al., 2014, **Supplementary Figure S1**). Long-term hydro-climatological records derived from regional tree-ring studies show a trend of declining precipitation from both the ISM and winter westerlies (Sano et al., 2012, 2017; Singh et al., 2019). However, winter precipitation has increased in recent decades (Treydte et al., 2006; Yadav et al., 2017). In contrast, tree-ring-derived regional temperature climatology shows an increasing trend irrespective of the season, with a prominent increase in the winter temperatures (Shah et al., 2019; Gaire et al., 2020; Panthi et al., 2021).

2.2 WCH Tree-Ring $\delta^{18}O$ Record

The tree-ring cellulose $\delta^{18}O$ records from three sites distributed across the studied region (**Figure 1**), comprising the dominant tree species (**Table 1**), were used to reconstruct the climatology of regional atmospheric humidity content (AMC). The first site (Manali: Sano et al., 2017) is located at the northwestern periphery of the ISM incursions. The second site (Uttarakashi: Singh et al., 2019) encompassed $\delta^{18}O$ records from three species belonging to two different plant functional types (PFTs) that differ in their phenological cycle (**Table 1**): one PFT included an evergreen conifer and the other was a broadleaf deciduous species

TABLE 1 | Tree-ring oxygen isotope datasets of different tree species used in this study (WCH: western-central Himalaya; CH: Central Himalaya; ECH: eastern central Himalaya).

No.	Sampling site	Region and coordinates	Tree species	Annual phenology	Period	Mean (± SD) ‰	Data source
1.	Manali	WCH: 32°13′ N, 77°13′ E;	*Abies pindrow*	Evergreen conifer	1768–2008	30.05 (± 1.48)	Sano et al. (2017)
2.	Uttarakashi	WCH: 30°50′ N, 78°43′ E;	*Abies pindrow*	Evergreen conifer	1743–2015	29.44 (± 1.77)	Singh et al. (2019)
			Picea smithiana	Evergreen conifer	1830–2015	28.07 (± 1.68)	
			Aesculus indica	Deciduous broadleaf (Apr-Sep)	1820–2015	25.74 (± 2.2)	
3.	Jageshwar	WCH: 29°38′ N, 79°51′ E;	*Cedrus deodara*	Evergreen conifer	1,621–2008	29.68 (± 1.35)	Xu et al. (2018)
4.	Humla	WCH: 29°51′ N, 81°56′ E;	*Abies spectabilis*	Evergreen conifer	1778–2000	25.16 (±1.67)	Sano et al. (2012)
5.	Ganesh	CH: 28°10′ N, 85°11′ E;	*Abies spectabilis*	Evergreen conifer	1801–2000	22.26 (± 1.19)	Xu et al. (2018)
6.	Bhutan	ECH: 27°59′ N, 90° 00′ E;	*Larix griffithii*	Deciduous conifer	1743–2011	19.24 (± 1.08)	Sano et al. (2013)

TABLE 2 | Correlation between central Himalayan tree-ring $\delta^{18}O$ with three PFTs from Uttarakashi ($p < 0.05$).

Uttarakashi	Manali	Jageswar	Humla	Ganesh	Bhutan
(Singh et al., 2019)	Sano et al. (2017)	Xu et al. (2018)	Sano et al. (2012)	Xu et al. (2018)	Sano et al. (2013)
Abies pindrow (Evergreen conifer)	0.75	0.67	0.23	0.20	0.26
Picea smithiana (Evergreen conifer)	0.69	0.56	0.50	0.52	0.26
Aesculus indica (Deciduous broadleaf)	0.60	0.55	0.50	0.57	0.31

(*Aesculus indica*). The growth period of *A. indica* (April to September) coincides with the warm-wet phase in the central Himalaya. The $\delta^{18}O$ records from the third site (Jageshwar: Xu et al., 2018) covered the longest period (~ 400 years) and similar to site one, were composed of a dominant conifer species (**Table 1**). Therefore, based on previous isotopic studies (Sano et al., 2017; Xu et al., 2018; Singh et al., 2019) and existing high inter-annual correlation among $\delta^{18}O$ records from WCH (**Table 2**), a ~400 years-long regional tree-ring $\delta^{18}O$ chronology was produced utilizing mean values of these records.

These studies followed standard sampling (two cores per tree) and dendrochronological procedures such as mounting, surface smoothing, tree-ring widths measurement, cross dating and quality control as per the standard methodology. Further, isolation of cellulose from whole wood and oxygen isotope analyses were carried out by the respective work within standard analytical precision and presented in the common δ-notation against VSMOW. For a detailed dendro-isotopic procedure one may refer to Sano et al. (2017), Singh et al. (2019) and Xu et al. (2018).

2.3 Reanalysis of Datasets

In-situ inter-annual meteorological records are mainly available for lower elevations (< 2000 m asl). Therefore, long-term temperature and precipitation datasets for the study region were obtained from CRU (TS.3.22, 0.5° x 0.5°, monthly, 1901–2015; Harris et al., 2014). The monthly reanalysis AMC dataset (0.5° x 0.625°) was obtained from MERRA-2 (i.e., total precipitable water vapour, http://giovanni.sci.gsfc.nasa.gov) from 1982–2015 ($n = 34$ years). Monthly soil moisture data, from 1982 to 2015, were obtained from the NOAA Climate Prediction Center (0.5° x 0.5°) (https://psl.noaa.gov/data/gridded/data.cpcsoil.html)

2.4 Satellite-Based Observations

MODIS: Regional trends in leaf area index (LAI: MOD15A2H) and evapotranspiration (ET: MOD16A2) since 2000 were deduced using 500 m resolution, 8-days composite MODIS products. Products were clipped using the shapefile for the WCH and pixel values were exported using ERDAS imagine to ASCII format. A MATLAB code was prepared to calculate the average LAI value of each image. LAI and ET computations were performed following the processing manual (www.reverb.echo.nasa.gov) (**Supplementary Table S1**). Regional sensitivity of ET to LAI ($\Delta ET/\Delta LAI$) was derived following Zeng et al. (2016).

LANDSAT: To detect changes in valley-scale vegetation area and greening trends (> 2,500 m asl), we utilized 30 m resolution L1T Landsat data since 1972 with different onboard sensors (MSS, TM, ETM + , OLI) (a total of 766 images, **Supplementary Table S1**). Changes in the seasonal vegetation area of eight evenly distributed glacial valleys in WCH (**Supplementary Table S2**) were derived during summer (April–September: when both evergreen and deciduous canopies are green) and winter (October–March: evergreen species only) from the NDVI (Normalized Difference Vegetation Index: > 0.3). The images were downloaded (https://glovis.usgs.gov), processed and analysed to detect multi-year seasonal vegetation trends. The watershed boundary of each valley (four valleys each in Garhwal Himalaya and Kumaun Himalaya: **Supplementary Table S2**) was delineated by utilizing mosaicked and re-projected tiles of 30 m Advanced Spaceborne Thermal Emission and Reflection Radiometer Global Digital Elevation Model v2 (http://gdex.-cr.usgs.gov/gdex/). Available L1T datasets with less than 10% cloud cover were selected and referenced to the Geographic Coordinate system UTM Zone 44N. In order to bring time-series data to a common scale, digital number values from each image were converted to

radiance using gain and offset values specified in the image metadata. Selected Landsat image were transformed into NDV time series using the following equation: $NDVI = \frac{NIR - Red}{NIR + Red}$ where "NIR" and "Red" are wavelengths in near-infrared and red bands, respectively. Five-year seasonal image composites, using maximum value composite procedure, were used, except for the period from 1972–1980, where a nine-year composite was generated due to limited availability of cloud-free images. This compositing process strongly reduces the effects of clouds, snow, seasonal differences caused by solar angle differences and noise. Reducing the data volume also minimizes errors in phenological changes.

CERES: Multi-year radiative forcing changes at the scale (Synoptic 1° × 1°; monthly; Product: EBAF-TOA 4.0) of the eight WCH glacial valleys (**Supplementary Table S2**) were observed with Cloud and Earth Radiation Energy System (CERES), one of the most important global satellite detectors to monitor radiation and energy budget. Net radiative forcing and its components (shortwave and longwave), at the surface (SFA), and at the top of the atmosphere (TOA) were downloaded from the official website (https://ceres.larc.nasa.gov/) at a monthly scale from March 2000 to December 2018. Longwave, shortwave, and net fluxes under clear and all-sky conditions were used to compute radiative forcing at the TOA and SFA following the equations (1 to 9) given in Bao et al. (2019) and details of the computation of radiation components can be found in the supplementary table (**Supplementary Table S3**).

2.5 Glacier Mass Balance Data

The present study utilized the tree-ring cellulose $\delta^{13}C$-derived proxy of annual glacier mass balance reconstruction over 273 years of four benchmark glaciers in the region (Singh et al., 2021a). This reconstruction is based on previous and relevant proxy-based glacio-hydrological studies, based on the assumption that climate indirectly connects the mass balance of a glacier with tree-ring C isotope ratios (Borgoankar et al., 2009; Shekhar et al., 2017; Zhang et al., 2019; Singh et al., 2021a). These four benchmark glaciers are *in-situ* monitored glaciers that are evenly distributed across the study region: Dokriani glacier (in DOK valley), Chorabari glacier (in MAN valley), Tipra Bamak (in CHA valley) and Dunagiri glacier (in NAN valley) (**Figure 1**; **Supplementary Table S2**).

2.6 Statistical Reconstruction and Analyses

To understand the relationship between atmospheric humidity (AMC) and hydroclimatic signal in evergreen conifers and broadleaf deciduous $\delta^{18}O$ data, simple Pearson correlations were applied with a response function approach. To investigate the correlations of $\delta^{18}O$ data with the monthly AMC averages in both cases, correlations were analysed at confidence intervals of 95% and 99%. In the case of evergreen conifers, response function analysis was performed from August of the previous growth year through to September of the current year. In the case of broadleaf deciduous species, with a growth cycle from April to September, the response function was performed for this period. To further corroborate the response functions, we plotted 3-month moving correlation coefficients between conifer $\delta^{18}O$ and mean AMC from 1982/1983 to 2014/2015 (**Table 3**).

Based on the above significant correlations, we established linear regression models for AMC reconstructions: 1) for previous year August to September (pAugest—September) based on $\delta^{18}O$ of regional conifers, and 2) for April to September based on $\delta^{18}O$ of the broadleaf deciduous species *A. indica*. Reconstructions were performed using the LM module in *R* (ggplot2 package, Wickham, 2016). After applying statistics to check the strength of our linear regression model (specifically, the F-test, residual standard error, root mean square error, Durbin–Watson test), we applied Akaike's and Bayesian information criteria for model evaluation and selection (**Table 3**). Therefore, a linear regression model was employed for the reconstruction of annual (pAugest—September) AMC over the past 395 years (1621–2015) and the corresponding empirical equation is:

$$AMC_{annual} = 27.392 - 0.487 \times \delta^{18}O_{regional\ conifers}$$

Here, $\delta^{18}O_{\text{regional conifers}}$ is the mean chronology of regional evergreen conifers and AMC is annual atmospheric moisture content (Kg m^{-2}). Detailed calibration–verification statistics are presented in **Table 3**, which indicate the strength and reliability of our reconstruction. Validation tests including the number of sign agreements between reconstructed series and observed AMC records, and cross-correlation between reconstruction and measurements were significant ($p < 0.001$).

Furthermore, a linear regression model was also employed for the reconstruction of summer season (April–September) AMC over the past 196 years (1820–2015) by utilizing $\delta^{18}O$ of a broadleaf deciduous species (*A. indica*). The corresponding empirical equation is:

$$AMC_{summer} = 25.885 - 0.388 \times \delta^{18}O_{deciduous}$$

Here, $\delta^{18}O_{\text{deciduous}}$ is chronology of *A. indica* and summer AMC is atmospheric moisture content (Kg m^{-2}) during April to September. Model and calibration–verification statistics indicate reliability and strength of this reconstruction model (**Table 3**). Validation tests including the number of sign agreements between the reconstructed series and observed AMC records, and cross-correlation between reconstruction and measurements are significant ($p < 0.001$). Finally, October to March (winter) AMC was estimated from the above reconstructions.

The leave-one-out cross-validation method (LOOCV; Michaelsen, 1987) was used for the entire calibration period (1982/1983–2014/2015) and verifying the reconstruction (**Table 3**). This method is most suitable when the length of observed records is short (Shekhar et al., 2017; Zhang et al., 2019; Singh et al., 2021a); each observation is successively withdrawn, and a model is estimated based on the remaining observations and a prediction is made for the omitted observations. The LOOCV analysis was performed using package "caret" (Kuhn, 2015). Statistics such as sign test, product mean test (PMT), reduction of error (RE), and correlation coefficients were calculated to evaluate the similarity between observed and estimated values (**Table 3**). The PMT and RE statistics provide

TABLE 3 | Statistics of calibration, and leave-one-out cross-validation (LOOCV) for April—September, and annual (Augest—September) AMC reconstructions.

Statistics of calibration [time span 1982/1983–2014/2015 C.E].	*r*	R^2	Adjusted R-squared	F-test	RSE	RMSE	AIC	BIC	DW
April-September AMC	–0.626**	0.392	0.372	20.01**	1.077	0.960	102.4	106.9	1.584*
Annual AMC	–0.671**	0.450	0.432	25.41**	0.715	0.637	75.47	79.96	1.242**
Leave-one-out cross-validation (LOOCV).	*r*	R^2	MAE	RMSE	ST (+/–)	PMT	RE	CE	DW
April-September AMC	–0.559**	0.313	0.878	1.112	27*+ / 6*–	1.394	0.299	0.450	1.405**
Annual AMC	–0.616**	0.380	0.604	0.737	26*+ / 7*–	2.202	0.459	0.298	1.191*

r: *correlation coefficient; R2, Coefficient of determination (R-squared) or variance explained; F, F-test, RSE: Residual standard error; MAE, Mean Absolute Error, RMSE: Root Mean Square Error; AIC, The Akaike information criterion; BIC, Bayesian information criterion; DW, The Durbin Watson; statistic ST, Sign-test sign; RE, reduction of error; CE, Coefficient of efficiency; PMT, Product mean test,* $^*p < 0.05$, $^{**}p < 0.001$.

a rigorous test of the association between actual and estimated series. Positive values indicate the predictive capability of the model. A positive RE is evidence of a valid regression model (Fritts, 1976). In addition, other statistics, viz., root mean square error, coefficient of efficiency, mean absolute error, and Durbin–Watson test were carried out to evaluate the linear regression model (**Table 3**). The reconstructions were standardized using Z-scores and smoothed with 11-years or 21-years fast Fourier transform to highlight the common climate signals. To understand regional scale-climatic features associated with present seasonal atmospheric moisture reconstruction, we performed cross-field spatial correlation with gridded seasonal precipitation (CRU TS 4.05) using KNMI Climate Explorer (http://climexp.knmi.ni; van Oldenborgh and Burgers, 2005).

3 RESULTS AND DISCUSSION

3.1 Coherent Tree-Ring $\delta^{18}O$ Chronologies of WCH

Tree-ring oxygen isotope ratio ($\delta^{18}O$) is a precise recorder of regional hydroclimatic condition (Baker et al., 2016). High temporal coherency between site-chronologies expands the spatial scale and increases the reliability of dendroclimatic reconstructions (Kahmen et al., 2011; Xu et al., 2017; Zeng et al., 2017; Xu et al., 2018). Moreover, the climatic sensitivity of tree ring $\delta^{18}O$ is further enhanced when high correlations among site-chronologies allow the combination of tree species of diverse functional types (e.g., Xu et al., 2018; Singh et al., 2019). Cellulose $\delta^{18}O$ chronologies have been extensively utilized to study the spatial climate heterogeneity over the HKT, covering century to millennium-scale variability in regional hydroclimate, e.g., changes in precipitation, atmospheric moisture, cloud cover, and vapor pressure (Treydte et al., 2006; Sano et al., 2012; Sano et al., 2013; Hochreuther et al., 2016; Grießinger et al., 2017; Sano et al., 2017; Xu et al., 2018; Huang et al., 2019; Singh et al., 2019; Managave et al., 2020).

As tree roots take up soil water without fractionation between the heavier and the lighter water molecules, therefore, a major part of the isotopic signature in tree rings should reflect the variation in precipitation or atmospheric humidity $\delta^{18}O$ (Baker et al., 2016; Lehmann et al., 2018; Lehmann et al., 2020; Managave et al., 2020). The mechanisms associated with physical fractionation of stable oxygen isotopes over lower latitudes indicate that tree-ring $\delta^{18}O$ values are mainly regulated by $\delta^{18}O$ of atmospheric humidity and are dominated by Rayleigh distillation *via* amount effect and or local moisture recycling (Baker et al., 2016). However, depending upon the atmospheric humidity condition, basin-intrinsic ecophysiological processes (e.g., isotopic composition of soil water, leaf-water enrichment, and oxygen isotope exchange reactions of photosynthates with water) may have a considerable effect on tree-ring $\delta^{18}O$values (Baker et al., 2016). Nevertheless, in the Himalayan environment with higher atmospheric humidity, tree-ring $\delta^{18}O$ records have been widely utilized to reconstruct century to millennium-scale variability in regional precipitation and hydroclimatology (Roden et al., 2005; Lehmann et al., 2018).

Over the central Himalaya, utilizing levels of correlations (0.11–0.94) among $\delta^{18}O$ chronologies of five sites, Xu et al. (2018) showed a decline in the strength of the ISM since the last 180 years. Moreover, $\delta^{18}O$ chronologies of different functional types (conifers and deciduous) from a WCH site (Uttarakashi) confirmed declining ISM precipitation in the region (Singh et al., 2019). These studies indicate that irrespective of site and tree species, interannual changes in ISM-derived atmospheric moisture are closely related to the El Niño–Southern Oscillation, but correlation strength varied synchronously across the central Himalaya (Sano et al., 2012; Sano et al., 2013; Sano et al., 2017; Xu et al., 2018; Singh et al., 2019).

However, our analyses of all six $\delta^{18}O$ records across the central Himalaya (**Table 1**) reveal a remarkable climatic distinction between the eastern (ECH) and western (WCH) part of the central Himalaya (**Supplementary Figure S2**). Studies even suggest increasing climatic heterogeneity over the last 6 decades (Singh et al., 2021a). Towards the eastern side, $\delta^{18}O$ records indicate normal ISM conditions during the 20th century (Bhutan: Sano et al., 2013; Hochreuther et al., 2016). In contrast, $\delta^{18}O$ chronologies from the central (Ganesh: Xu et al., 2018) and western regions (WCH) (Manali: Sano et al., 2017; Uttarakashi: Singh et al., 2019; Jageshwar: Xu et al., 2018; and Humla: Sano et al., 2012) unanimously show declining monsoon precipitation, as reflected in enriched tree-ring $\delta^{18}O$ values (**Figure 2**). More specifically, mean values of $\delta^{18}O$ chronologies progressively decline eastwards with a substantial difference (8‰–10 ‰) between the Bhutan site (19.24 ‰) and WCH chronologies (29.31 ‰) (except Humla) (**Table 1**, **Supplementary Figure S2**). This difference likely indicates a

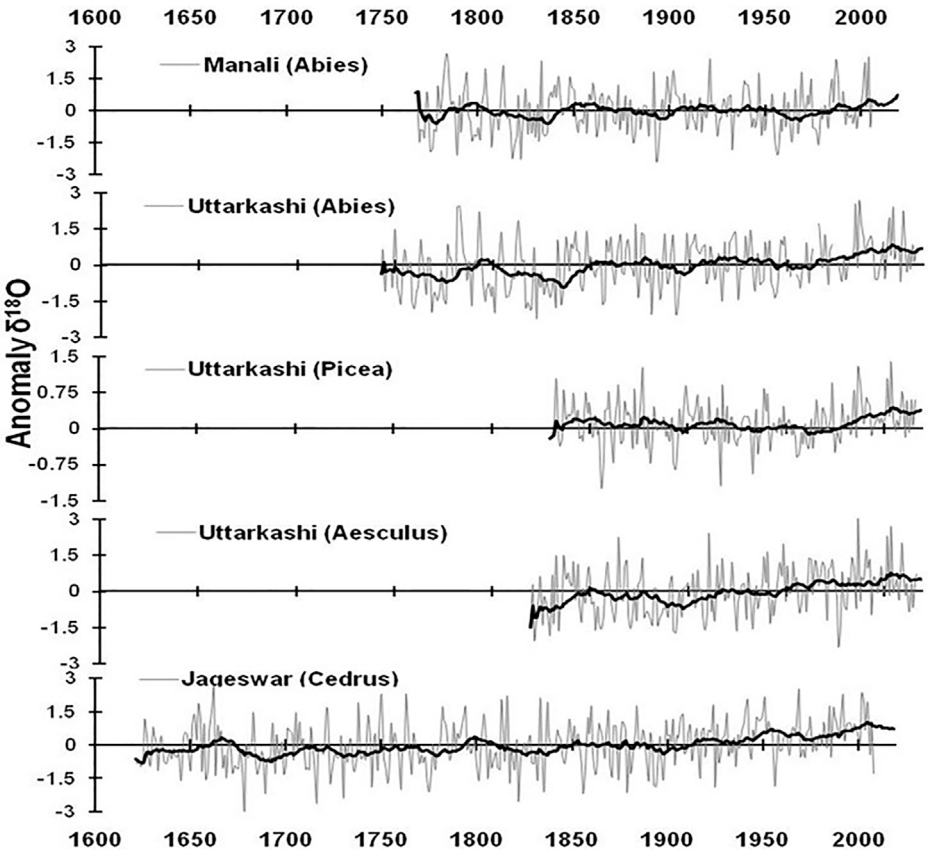

FIGURE 2 | Anomalies (Z scores) of highly coherent site-chronologies from the study region (WCH) (Manali: Sano et al., 2017; Uttarakashi: Singh et al., 2019; Jageshwar: Xu et al., 2018). Dark lines denote 21-years moving averages.

greater influence of the Bay of Bengal branch of the ISM on the eastern Himalaya (Perry et al., 2020; Singh et al., 2021a). A correlation matrix of six central Himalayan site chronologies found remarkably high correlations (0.55–0.75) among the WCH chronologies (Manali: Sano et al., 2017; Uttarakashi: Singh et al., 2019 and Jageshwar: Xu et al., 2018). However, inclusion of the Humla $\delta^{18}O$ chronology (Sano et al., 2012) substantially lowers the correlation (0.23–0.5) (**Table 2**). Therefore, this study utilizes only the coherent WCH chronologies to reconstruct the regional changes in AMC. The WCH $\delta^{18}O$ record spanning the last four hundred years indicates a prominent shift towards a drier phase after the 1960 s (**Figure 2**). This recent drier phase in regional hydroclimate has generally been attributed to anthropogenic emission-induced warming and resultant reduced land–ocean thermal contrasts (Xu et al., 2018).

3.2 Hydroclimate-Response Function

The Pearson correlations with a response function approach showed the relationship between atmospheric humidity (AMC) and hydroclimatic signal in evergreen conifers and broadleaf deciduous $\delta^{18}O$ data. The response function analysis for evergreen conifers from August of the previous growth year to September of the current year (pAugest-September) revealed a significant negative correlation ($r = -0.671$; $p < 0.001$). However, during peak winter (December and January) the correlation was positive (**Figure 3A**). Previously, a positive correlation with winter atmospheric humidity was observed in the study region. The correlations for these winter months were negative with the precipitation (Sano et al., 2012; Sano et al., 2017; Xu et al., 2018; Singh et al., 2019). A time lag induced by winter snowfall and frozen conditions could plausibly explain this consistent behaviour across the study region. Moreover, to corroborate the response function, we plotted 3-month moving correlation coefficients between evergreen conifer $\delta^{18}O$ and mean AMC from 1982/1983 to 2014/2015. This enhanced the correlations considerably, even in the winter months (**Figure 3B**).

In the case of broadleaf deciduous tree species, having an annual growth cycle between April and September, the response function analysis showed a significant correlation ($r = -0.63$; $p < 0.001$) (**dsl**). Three-month moving correlation coefficients between deciduous $\delta^{18}O$ and mean AMC improved the relationship substantially. This is in parity and has been shown with 3-month moving averages of growing season LAI dynamics, the correlation between ET and LAI, and the sensitivity of ET to LAI ($\Delta ET/\Delta LAI$: mm day^{-1} (m^2 m^{-2}) (**Figure 3D**). This indicates that the above biophysical parameters including their sensitivity remain tightly coupled to active vegetation growth from April to September. In contrast, for the non-growing winter season months, the sensitivity of ET to LAI, in particular, remained low and decoupled.

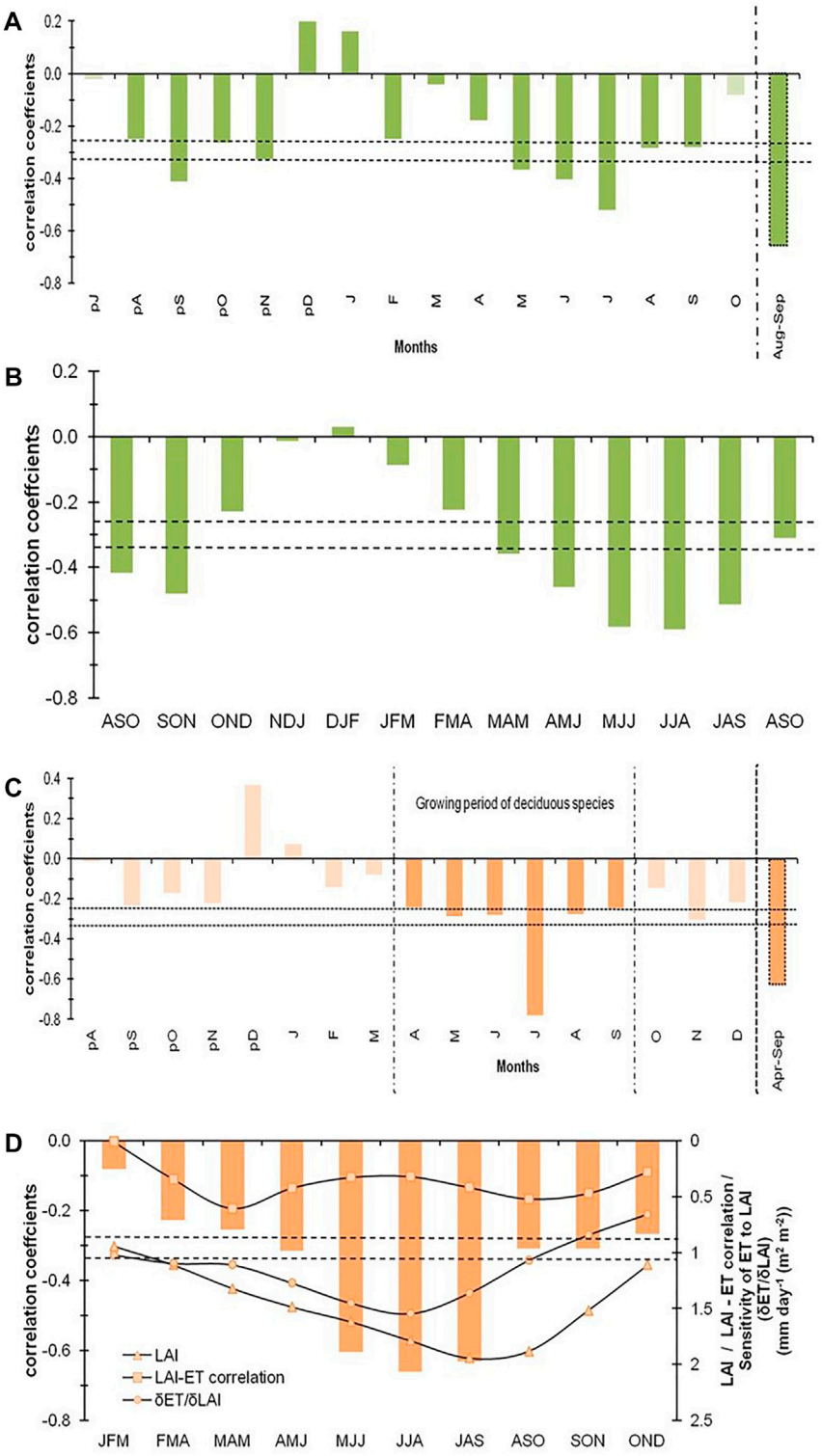

FIGURE 3 | (A,B). Hydroclimatic response-function for the evergreen conifers. **(A)** Monthly correlations between regional conifer $\delta^{18}O$ chronologies with atmospheric moisture content (AMC), **(B)** Three-month moving correlation coefficients between regional conifer $\delta^{18}O$ chronologies and AMC, The dotted horizontal lines indicate the 950025 and 99% confidence level respectively. Prefix "*p*" before the months denotes the months of the previous growth year. **(C,D)**. Hydroclimatic response-function for the deciduous species. **(C)** Monthly correlations between broadleaf deciduous $\delta^{18}O$ chronology with AMC, and **(D)** Three-month moving correlation coefficients between broadleaf deciduous $\delta^{18}O$ chronology with AMC. It has been shown with three-month moving average of leaf area index (LAI), correlation between evapotranspiration (ET) and LAI, and the sensitivity of ET to LAI [$\Delta ET/\Delta LAI$: mm day^{-1} (m^2 m^{-2})]. The dotted horizontal lines indicate the 95% and 99% confidence level respectively. Prefix "*p*" before the months denotes the months of the previous growth year.

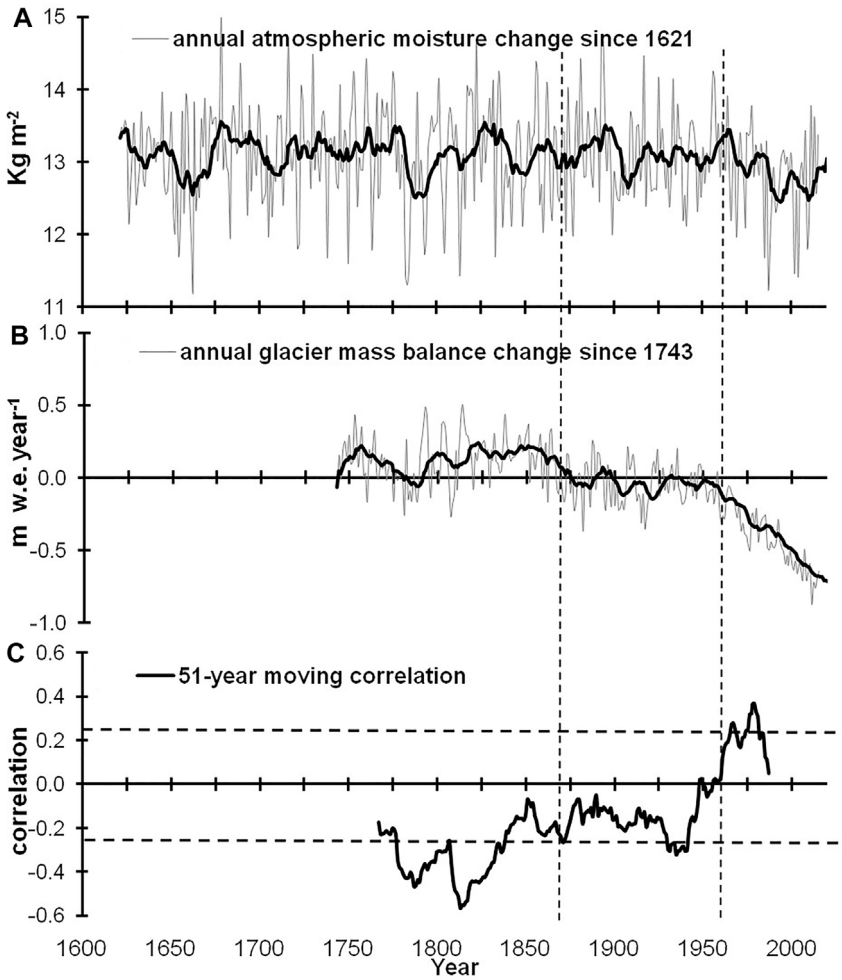

FIGURE 4 | (A) Annual (pAug—Sep) AMC reconstruction derived from regional (WCH) conifer $\delta^{18}O$ chronologies (except deciduous species) since 1,621–2,015 CE, **(B)** 273-years of glacier mass balance (GMB) variability reconstructed utilizing cellulose $\delta^{13}C$ records of WCH (Singh et al., 2021a), and **(C)** Low-frequency temporal variations (51-years running correlations) between annual AMC and GMB. The dotted horizontal lines indicate the 95% confidence level. Dark lines denote 11-years moving average. Vertical dashed lines are the results of break-point analysis.

3.3 Four Centuries of Regional Atmospheric Moisture Dynamics

The correlation ($r = -0.671$, $p < 0.001$, $n = 34$) between WCH conifer $\delta^{18}O$ chronologies and observed AMC was strong enough to establish a significant calibration model. A linear regression model was thus employed for the reconstruction of annual AMC (pAugest–September) over the past 395 years (1621–2015). The equation accounts for 45% of the AMC variance during the observation period (1982–2015) (**Table 3**; **Figure 5B**).

Smoothing of resultant annual AMC reconstruction with an 11-years moving average and break-point analyses indicates decreasing atmospheric moisture since the mid-19th century and a prominent decline in recent decades (since the 1960 s) (**Figure 4A**). Our results on seasonal disaggregation of annual AMC indicate that the decline in moisture influx in the region could be ascribed to both major atmospheric circulations, i.e., the ISM and the westerly circulation (**Figure 5**). Paleoclimatic evidence such as tree-ring $\delta^{18}O$ chronologies (Sano et al., 2012; Sano et al., 2013; Sano et al., 2017; Xu et al., 2018; Singh et al., 2019), speleothems (Kotlia et al., 2012; Liang et al., 2015) and ice-core records from the central Himalaya (Kaspari et al., 2008) show that regional hydroclimate shifted towards a drier phase from the mid-19th century onwards. Studies indicate a reorganisation of hemispheric atmospheric circulation following the Little Ice Age. Moreover, a recent decline in AMC (since the 1960 s) could be attributed to increasing temperatures and climate change (Xu et al., 2018).

3.4 Seasonal Reconstructions of Atmospheric Moisture

An approximately three hundred year-long glacier mass balance (GMB) variability record comprising four benchmark glaciers of WCH has previously been reconstructed based on cellulose $\delta^{13}C$ records of two regionally dominant evergreen conifer tree species

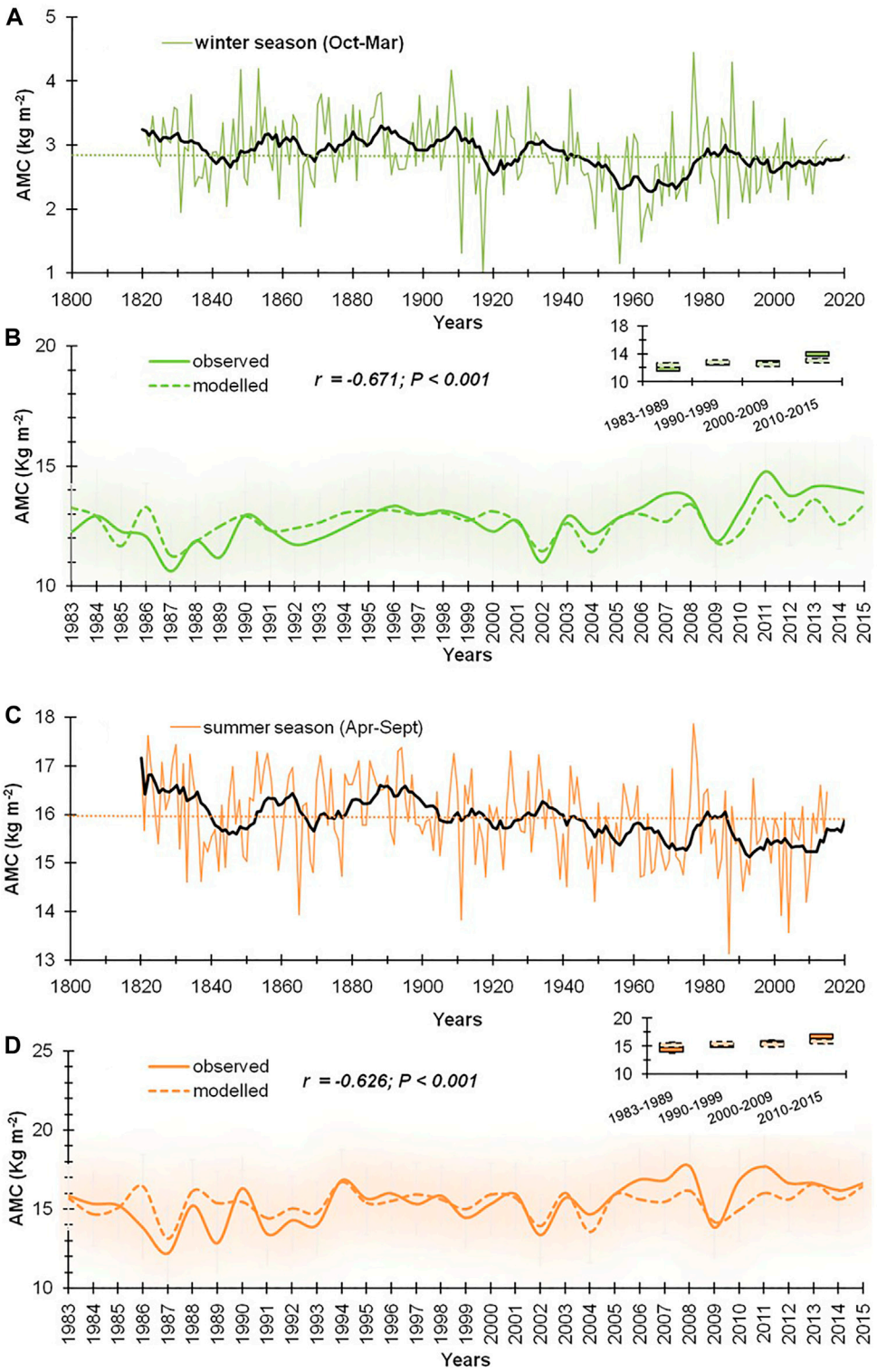

FIGURE 5 | (A,B). **(A)** Winter season (Oct—Mar) atmospheric moisture dynamics over the study region (WCH) since 1820 CE derived as difference between annual and summer season AMC. Dashed green horizontal line indicates long-term mean, while solid black line is 11-years moving average. **(B)** Comparison plot of observed and reconstructed annual AMC with regional conifer $\delta^{18}O$ chronologies. Inset plot indicates inter-annual coherence, while shades denote 95% prediction limit **(C,D)**. **(C)** 196-years record of summer season (April—September) atmospheric moisture dynamics over the study region (WCH). Dashed orange horizontal line indicates long-term mean, while solid black line is 11-years moving average. **(B)** Comparison plot of observed and reconstructed summer-season AMC with broadleaf deciduous $\delta^{18}O$ chronology. Inset plot indicates inter-annual coherence, while shades denote 95% prediction limit.

(*Abies pindrow* and *Picea smithiana*) (Singh et al., 2021a) (**Figure 4B**). We show the multi-decadal coherence between GMB and AMC. Over the common record of 273 years, the 51-years moving correlations between atmospheric moisture and ice mass display a shift in the relationship since the mid-19th century, which became even more pronounced after the 1960 s (**Figure 4C**).

To find the cause of this shift in the AMC—GMB relationship, we disaggregated annual AMC on a seasonal scale (summer and winter accumulation seasons). Approximately 200 years (1820–2015) of AMC record of the summer accumulation season (April–September) was derived based on a dominant deciduous tree species (*A. indica*) that completes its annual phenological cycle between April and September and remains physiologically dormant during winter (**Figures 3C,D**) (Singh et al., 2021a). As discussed above, a strong correlation ($r = -0.626$, $p < 0.001$, $n = 34$) was observed with summer season AMC (1982–2015) and the corresponding equation accounted for 39% of the AMC variance during the observation period. Further, model calibration–verification and validation tests statistics (**Table 3**) indicate the strength of the reconstruction. Thus, the winter season (October–March) AMC was derived from the annual and summer season AMC.

3.4.1 Winter Season Moisture Record From the Last Two Centuries

Here, we present a new reconstruction of AMC over the WCH during the winter season (October–Mar), which provides baseline data from the western transitional region in the central Himalaya and an opportunity to assess its relationship with regional hydroclimatic records (such as precipitation, temperature, snowfall and river flow). Our record of winter season AMC over almost two centuries indicates relatively stable condition prior to the 1920s, a period of decline between the 1920s and 1960s, and a revival of moisture influx driven by winter westerlies in the region since the 1970s (**Figure 5A**). The reconstructed AMC is remarkably similar to a tree-ring $\delta^{18}O$-derived millennium-scale precipitation record from the high mountains of northern Pakistan, where annual precipitation is dominated by westerly synoptic fronts (Treydte et al., 2006). Winter season AMC over the WCH and precipitation in northern Pakistan showed a high inter-decadal coherence during the common period. The trend of the wet condition in the later part of the 20th century is remarkably similar in both reconstructions. Similarly, Yadav et al. (2017) also noted the moist condition since the 1970s in the Karakorum and the westerly-dominated Indian northwest Himalaya. Their observed decline in tree-ring width-derived hydroclimatic index during the early 20th century (Yadav et al., 2017), is consistent with our AMC record. Recent enhanced moisture influx in the region from mid-latitude westerlies has been ascribed to the strengthening of western disturbance (Yadav et al., 2017), or possibly anthropogenic influences on acceleration of the hydrological cycle (Treydte et al., 2006). In addition, several regional hydroclimatic records (precipitation, snowfall, river flow) substantiate our reconstruction (Bhutiyani et al., 2008; Bhutiyani et al., 2010; Cook et al., 2013; Singh and Yadav, 2013; Yadav and Bhutiyani, 2013). The decades of low AMC, viz., 1840s, 1870s, 1910–1920s, and 1960–1970s, are consistent with the negative anomaly in the regional hydroclimatic index (Yadav et al., 2017), low snowfall and flow in the Indus River (Cook et al., 2013; Yadav and Bhutiyani, 2013). River flow of the Indus and regional snowfall were relatively high in the 1890s, 1980s, and 1990s when AMC was high in our reconstruction. The low AMC values recorded during the 1960–1970s are consistent with low winter flow in the Satluj River (Bhutiyani et al., 2008; Singh and Yadav, 2013). The 20th century low and high AMC episodes in our reconstruction have also been observed in instrumental winter precipitation and snowfall records from the western Himalaya (Bhutiyani et al., 2010; Yadav and Bhutiyani, 2013). The consistency in the decadal coherence between winter temperature reconstructions from the central Himalaya (Shah et al., 2019; Gaire et al., 2020; Panthi et al., 2021) and our AMC records is remarkable (Wang et al., 2020). Moreover, to understand regional-scale climatic features and to validate our results associated with present winter season AMC reconstruction, we performed cross-field spatial correlation with gridded winter season precipitation (CRU TS 4.05). The spatial correlation calculated for the peak winter months (December and January) over the period of 1901–2014, showed a significant positive correlation with westerly dominated regions of the HKT orogeny (**Supplementary Figure S3a**).

3.4.2 A Summer Season Record of Atmospheric Moisture

Similar to winter season AMC, our new record of summer-accumulation season (April to September) AMC is substantiated by regional hydroclimatic records. As discussed previously, summer season AMC ($r = -0.626$, $p < 0.001$, $n = 34$) is based on a regionally-dominant deciduous tree species (*A. indica*). Related dendrochronological statistics (calibration–verification and validation tests) indicate the strength of this reconstruction (**Table 3**). This record of about two centuries of AMC indicates a consistent summer monsoon-driven moisture influx decline in the region since, at least, the beginning of the 20th century. This result also underlines higher AMC levels during the 19th century, with major fluctuations (**Figures 5C,D**). Broadly, all summer-monsoon season hydroclimatic records from the central Himalaya (Sano et al., 2012; Sano et al., 2017; Xu et al., 2018; Singh et al., 2019) corroborate our AMC reconstruction. Studies unanimously indicate a weakening trend in the ISM circulation since the late 19th century or early 20th century (Singh et al., 2019). Even decadal to inter-decadal patterns of our reconstructed series are consistent with available hydroclimatic records, e.g., the decades of low summer season AMC, viz., 1840s and 1870s. Moreover, regional studies based on ice-cores and tree-ring $\delta^{18}O$ from the core monsoon-zone of the Himalaya show a similar trend (Zhao and Moore, 2006; Kaspari et al., 2008; Liu et al., 2013; Liu et al., 2014; Wernicke et al., 2017). These records reveal a spatially coherent signal and serve as a validation test of the

accuracy of our AMC reconstruction. In particular, tree-ring and speleothem $\delta^{18}O$ records (Kotlia et al., 2012; Sano et al., 2012; Liang et al., 2015; Sano et al., 2017; Xu et al., 2018; Singh et al., 2019) from our study region appear consistent with our reconstruction. In addition, to investigate regional-scale climatic features and to validate our results associated with present summer season AMC reconstruction, we performed cross-field spatial correlation with gridded summer season precipitation (CRU TS 4.05). The spatial correlation calculated for the summer months over the period (1901–2014), showed a significant positive correlation with the Arabian branch of the ISM dominated region (Singh et al., 2019) (**Supplementary Figure S3b**).

3.5 Temporal Correlation Between Ice Mass and Seasonal Atmospheric Moisture

3.5.1 Winter Season Atmospheric Moisture Content and Mass Balance

The low frequency (51-years) moving correlations between regional ice mass and atmospheric moisture during the winter season (October-March) showed high and significant variations in the common period of about two hundred years (**Figure 6A**). These varying relationships indicate high sensitivity to winter season atmospheric moisture variability. For example, prior to 1910s, during winter pluvial conditions (winter AMC remained above the long-term mean) (**Figure 5C**), the correlations remained positive but stable. During the stint of moisture decline up to the 1970s, the correlations significantly turned positive. Again, the correlations declined with the revival of winter westerlies after the 1970s (**Figure 6A**). The increasing regional winter temperatures since the last few decades (Shah et al., 2019; Gaire et al., 2020; Panthi et al., 2021) and a decadal consistency in the temperature - moisture covariability (Wang et al., 2020) could be the reason of sudden negative correlations. Overall, this behaviour probably indicates a high sensitivity of ice mass balance to the winter-westerlies in the region. In this context, winter-westerlies primarily determine the ice mass variability at the decadal timescales (Molg et al., 2014; Kumar et al., 2019; Khan et al., 2020; Singh et al., 2021a). Therefore, we contend that caution should be applied when referring to the glaciers in WCH as predominantly ISM-regulated or summer-accumulation type glaciers.

3.5.2 Summer Season AMC and Mass Balance

Unlike the winter season AMC—mass balance relationship, the 51-years moving correlations with summer season AMC indicated statistically insignificant variations in the common period of about two hundred years (**Figure 6B**). These relatively stable relationships probably indicate a low sensitivity of ice mass to atmospheric moisture variability during the summer season.

However, looking at the inter-decadal variation trends (**Figure 6B**), the correlations remained negative till the late 19th century, when our result and regional hydroclimatic records indicated pluvial condition. The correlations turned positive (though insignificantly) with a decline in ISM moisture influx in the region since the 20th century (Kotlia et al., 2012; Sano et al., 2012, 2017; Liang et al., 2015; Xu et al., 2018; Singh et al., 2019).

Moreover, it is interesting to note that despite a further and strong decline in ISM precipitation since the mid-20th century (**Figure 2**), the stability of the correlations is remarkable (**Figure 6B**). Therefore, it is highly possible that decadal-scale greening (Shen et al., 2015; Silva et al., 2016; Parida et al., 2020; Sigdel et al., 2020) with consequent increase in evapotranspiration (Singh et al., 2021b) and pre-monsoon precipitation in the region since the mid-20th century (Singh et al., 2006) might have compensated for the ISM precipitation deficit that helped to lower down and maintain the correlation (**Figure 6B**).

In support of the above hypothesis, we found a stronger correlation of WCH $\delta^{18}O$ values against evapotranspiration (R^2 = 0.48, $p < 0.001$, n = 15: 2000–2015) and atmospheric moisture content (R^2 = 0.38, $p < 0.001$, n = 34: 1982–2015) as compared to regional soil moisture (R^2 = 0.13, $p < 0.05$, n = 34: 1982–2015). These relationships point towards a dominant role of vegetation ecophysiology (stomatal control) in regulating atmospheric moisture (Kahmen et al., 2011; Singh et al., 2014). Earlier studies (Baker et al., 2016) also found that in a typical warm-moist environment (e.g., tropical rainforest), basin-intrinsic ecophysiological processes also have a control on $\delta^{18}O$ values. Further, a detailed and long-term investigation on isotopic composition of precipitation over the glaciers in our study region, particularly higher d-excess value suggests the importance of evapotranspiration and local moisture recycling (Verma et al., 2018).

Several studies consistently confirm that the recent increase in pre-monsoon precipitation is regional in nature (Karki et al., 2017; Talchabhadel et al., 2018; Shrestha et al., 2019). Higher temperatures increase the water holding capacity of the atmosphere according to the Clausius–Clapeyron relation, and further increase the evaporation from soil, glacial lakes, permafrost-active layer, and melted water. Modelling studies have also found that October to March atmospheric moisture have a positive feedback on ISM through large-scale circulation changes (Agrawal et al., 2019). Moreover, we comprehend that the reported decline in pre-monsoon surface temperature since the 1960s (Yadav et al., 2004) and concurrent increasing trend in pre-monsoon precipitation could be a consequence of evaporative cooling associated with regional vegetation greening (Shen et al., 2015). Multi-century temperature reconstructions from the adjacent western Nepal Himalayan region have also indicated that there is no increase in pre-monsoon temperature trends (Thapa et al., 2015; Aryal et al., 2020).

In the Himalaya-Tibet orogen, moisture recycling studies suggest a strong vegetation-precipitation feedback loop and high moisture recycling (Dirmeyer et al., 2009; Tuinenburg et al., 2012; Harding et al., 2013; Keys et al., 2016; Wang et al., 2020). The isotopic moisture recycling studies in the orogen too have indicated high moisture recycling rates and an enhancement in trends in recent decades (Joswiak et al., 2013; An et al., 2017). Modelling experiments further confirm that vegetation-mediated moisture recycling is a major source of atmospheric water vapour and precipitation particularly during

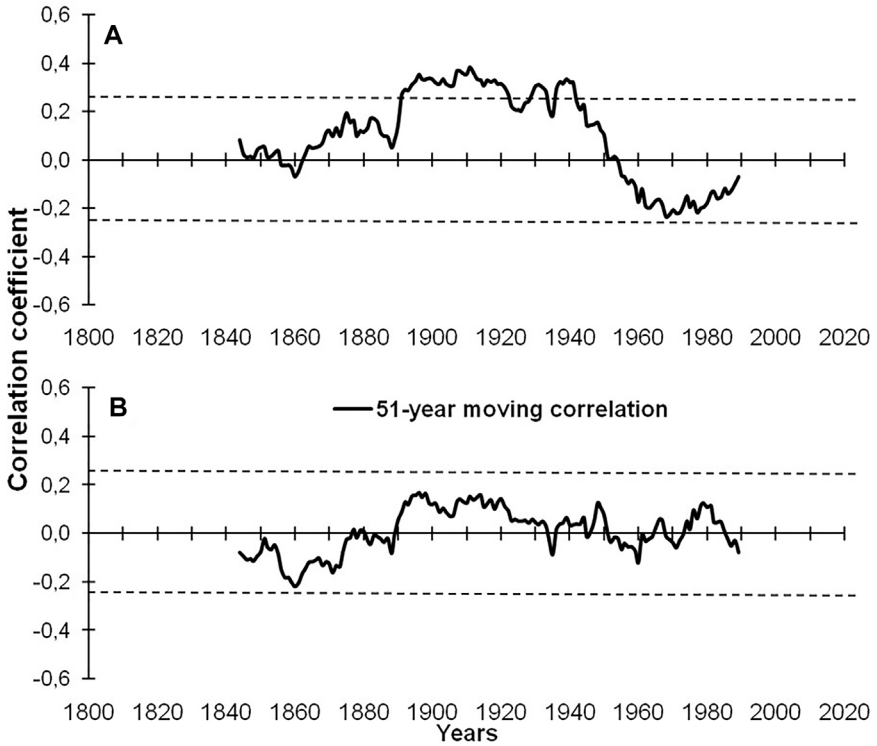

FIGURE 6 | (A) Low-frequency temporal correlations (51-years running correlations) between annual GMB and winter-season (October—March) AMC. **(B)** Low-frequency temporal correlations between annual GMB and summer-season (April—September) AMC. The dotted horizontal lines indicate the 95% confidence level.

the pre-monsoon season, when horizontal moisture transport is minimal.

3.6 Decadal Trends in Greening and Radiative Balance Analyses

A decadal-scale change in the vegetation is expected to modulate the regional radiative energy balance (McPherson, 2007). Numerous observations from the orogen have indicated a widespread greening and vegetation expansion including in the subnival vegetation (Shen et al., 2015; Silva et al., 2016; Anderson et al., 2020; Parida et al., 2020; Sigdel et al., 2020). In this context, we focussed at the glacial valley scale vegetation trend in WCH through MODIS (250 m; 2000–2015) and 5 decades (1970–2016) of Landsat imageries (30 m) (**Supplementary Table S2**). Analyses indicate a differential greening behaviour in the plant functional types. The deciduous vegetation coverage has expanded rapidly (37.2 km^2 yr^{-1}) compared to conifers (13.7 km^2 yr^{-1}) (**Supplementary Figure S4**). Results of Landsat imageries corroborated a rapid increase in deciduous vegetation with respect to evergreen conifers at the valley-scale (**Supplementary Figure S5**). On average, deciduous vegetation coverage increased by 24% (15%–35%) relative to the pre-1994 level across the WCH glacial valleys. Current mean deciduous coverage area in the valleys is 36%, varying between 22% and 49% in different valleys. Furthermore, both MODIS- and Landsat-derived seasonal green area coverage estimates indicate that approximately 40% (30%–50%) of the glacial valley area rapidly turns-up green with deciduous canopy development (April—May) (**Supplementary Figures S4, S5**).

Decadal-scale environmental changes resulting from warming, augmented moisture and nutrient flow from snow-glacier melting, enhanced pre-monsoon rainfall, and disturbances such as forest fires might have favoured the expansion of deciduous species. Thus, given widespread greening and thermophilization (a preferential expansion of broadleaf deciduous vegetation over evergreen conifers), we contend comprehensive changes and a gross-scale alteration in surface–atmosphere interactions having direct implication on regional radiative balance. In addition, favoured expansion of deciduous vegetation on the valley slopes may even have repercussions on seasonal radiative balance, as deciduous species remain leafless throughout the winter and rapidly turn green with the advent of the spring season.

The above factors and associated changes in albedo, canopy conductance, aerodynamic properties and atmospheric moisture flux are expected to perturb the regional radiative balance. Therefore, the CERES radiation dataset (2000–2018) covering glacial valleys in the WCH region was utilized to access shortwave (SRF), longwave (LRF) and net radiative forcing (NRF). Multi-year monthly average NRF at both the surface and at the top of the atmosphere (TOA) showed unimodal annual behaviour (**Figure 7**). NRF at TOA showed a maximum cooling effect (−45 to −55 W m^{-2}) during the monsoon months and remained below −25 W m^{-2} during the rest of the months. Interestingly, surface NRF from October to

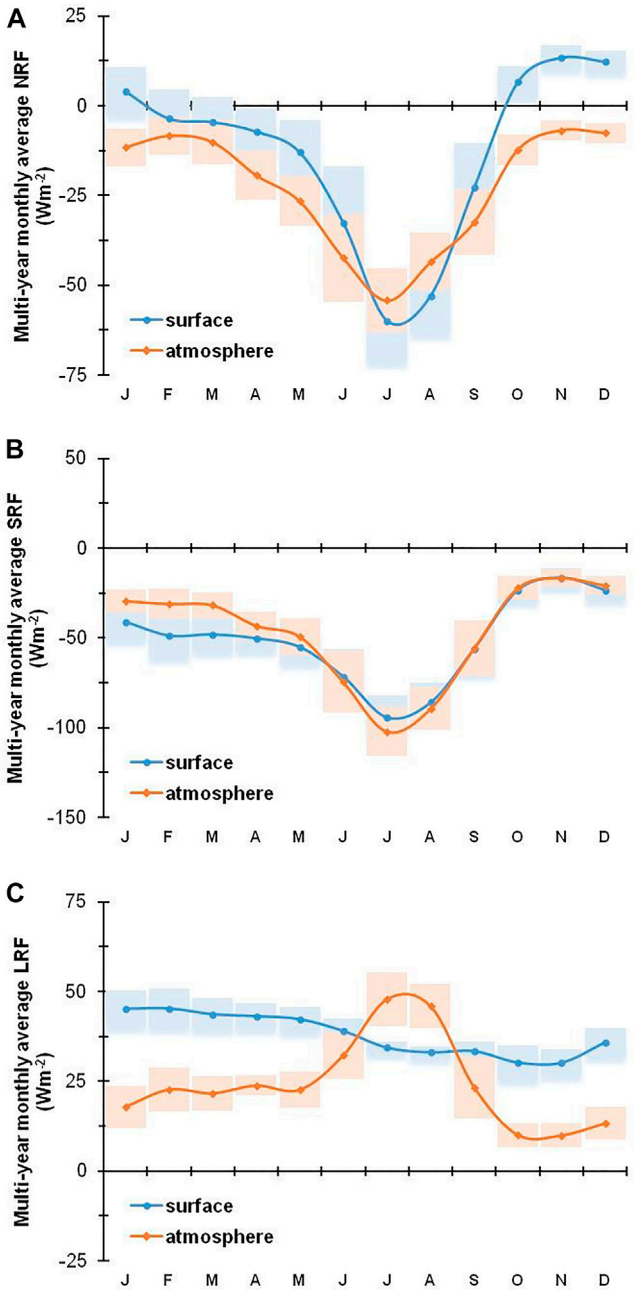

FIGURE 7 | CERES radiation dataset (2000–2018) covering eight glacial valleys in the WCH region (**Supplementary Table S2**) showing **(A)** net radiative forcing (NRF), **(B)** shortwave radiative forcing (SRF) **(C)**, and longwave radiative forcing (LRF), at both surface and atmosphere. Monthly standard deviation is indicated in respective colour.

May (except monsoon months) indicates a heating effect or a feeble cooling (**Figure 7**).

Further, we performed seasonal-scale analyses. During the post-monsoon to winter season, NRF at TOA indicated a cooling effect (−5 and −20 W m^{-2}). In contrast, surface NRF indicated net heating (1.0–10 W m^{-2}). Similarly, during spring or pre-monsoon season, NRF at TOA remained between −10 and −30 W m^{-2}, while surface NRF indicated a weak cooling (0.6–14 W m^{-2}). However, with the advent of the monsoon, both TOA and surface NRF resumed a cooling effect (**Figure 7**). Annual SRF (at both the surface and TOA) showed unimodal behaviour with a net cooling effect showing peak cooling (−70 to −100 W m^{-2}) during the summer monsoon months. Interestingly, the magnitude (−15 and −50 W m^{-2}) of TOA and surface SRF remarkably deviated during winter to pre-monsoon seasons with a mean difference of 5–10 W m^{-2} (**Figure 7**). Annually, LRF at both the surface (38 W m^{-2}) and TOA (24 W m^{-2}) had a heating effect. Across the seasons, the magnitude of surface LRF varied slightly (monsoon: 30 W m^{-2}; winter to pre-monsoon: 45 W m^{-2}). In contrast, LRF at TOA showed a unimodal behaviour with maximum heating (45–50 W m^{-2}) during the monsoon season and comparatively less heating (10–20 W m^{-2}) during winter to pre-monsoon seasons. These results, particularly radiative alterations from winter to pre-monsoon, suggest it is highly possible that enhanced winter season humidity coupled with winter warming (Shah et al., 2019; Gaire et al., 2020; Panthi et al., 2021) makes the environmental conditions favourable for vegetation growth in the following growing season (Huang et al., 2022).

These multi-year results indicate that the ongoing changes in vegetation albedo and in ecohydrology deserve future analyses to fully understand the impact of the vegetation changes on local and regional climate. In particular, it would be worth exploring the possibility that the energy increasingly released as latent heat by the expanding vegetation is subsequently advected and released at a higher elevation during condensation, favouring snowmelt (Harder et al., 2017). Additionally, the effects of the increased cloudiness associated with increased evapotranspiration (Duveiller et al., 2018) have to be evaluated in terms of the energy budget.

4 CONCLUSION

Warming-induced acceleration in the hydrological cycle could have an immediate implication on regions with strong land-atmosphere coupling such as the Himalaya. In this study, we present the first tree-ring isotope-derived hydroclimate and glacier interaction over the western transitional climate region of the central Himalaya. We utilized highly coherent, multi-species tree-ring oxygen isotope chronologies to derive regional changes in atmospheric moisture over the last four centuries. Our reconstruction implies decreasing annual precipitation or atmospheric moisture since the mid-19th century and a prominent decline in recent decades (since the 1960s). Annual atmospheric moisture was further resolved on a seasonal-scale by utilizing an oxygen isotope record of a dominant broadleaf deciduous species. This helped to create a unique record of atmospheric moisture during the winter season (October–March) and baseline data from this transitional climate zone. Our result confirms the revival of winter westerlies-driven moisture influx in the region since the 1970s. Another reconstruction of approximately two centuries of atmospheric moisture during the summer season (April-September) indicates a gradual decline in moisture influx from the beginning of the 20th century. Low-frequency temporal correlations (51-years running correlations) between regional hydroclimate and

ice mass balance indicate an abrupt phase-shift since the 1960s in a common record of 273 years. Our results specify that winter-westerlies rather than summer precipitation from ISM govern ice-mass variability in the WCH region. The study indicates that the attribution of ice mass to large-scale dynamics is likely to be modulated by local vegetation changes. We contend that glacier-climate models that account for these processes and feedback should include these findings to reliably improve the projections.

DATA AVAILABILITY STATEMENT

The raw data supporting the conclusion of this article will be made available by the authors, without undue reservation.

AUTHOR CONTRIBUTIONS

NS analyzed the final dataset and wrote the first draft of the manuscript. MS performed reconstructions and respective analyses. Satellite observations and respective analyses were performed by BP, VS, and RK. LM supervised the analyses and contributed to the interpretation. All authors contributed to writing, discussion and editing of the manuscript.

FUNDING

This publication is benefitting from the fund dedicated to Open Access publications of the Free University of Bolzano Library.

ACKNOWLEDGMENTS

NS acknowledges the DST (Govt. of India) for support under the Fast-Track Young Scientist Fellowship (File No. SR/FTP/ES-166/2014) and from the EUREGIO funded ASTER project, EGTC European Region Tyrol-South Tyrol-Trentino—IPN 101-32 and Austrian Science Fund (FWF). MS expresses gratitude to Dr. (Mrs.) Vandana Prasad (Director, BSIP, Lucknow). AG thanks the DST (Govt. of India) for the Sir J. C. Bose Fellowship (No.SR/S2/JCB-80/2011).

SUPPLEMENTARY MATERIAL

The Supplementary Material for this article can be found online at: https://www.frontiersin.org/articles/10.3389/feart.2022.868357/full#supplementary-material

REFERENCES

Agrawal, S., Chakraborty, A., Karmakar, N., Moulds, S., Mijic, A., and Buytaert, W. (2019). Effects of Winter and Summer-Time Irrigation Over Gangetic Plain on the Mean and Intra-Seasonal Variability of Indian Summer Monsoon. *Clim. Dyn.* 53 (5-6), 3147–3166. doi:10.1007/s00382-019-04691-7

An, W., Hou, S., Zhang, Q., Zhang, W., Wu, S., Xu, H., et al. (2017). Enhanced Recent Local Moisture Recycling on the Northwestern Tibetan Plateau Deduced from Ice Core Deuterium Excess Records. *J. Geophys. Res. Atmos.* 122 (23), 12–541. doi:10.1002/2017jd027235

Anderson, K., Fawcett, D., Cugulliere, A., Benford, S., Jones, D., and Leng, R. (2020). Vegetation Expansion in the Subnival Hindu Kush Himalaya. *Glob. Change Biol.* 26 (3), 1608–1625. doi:10.1111/gcb.14919

Aryal, S., Gaire, N. P., Pokhrel, N. R., Rana, P., Sharma, B., Kharal, D. K., et al. (2020). Spring Season in Western Nepal Himalaya Is Not Yet Warming: A 400-Year Temperature Reconstruction Based on Tree-Ring Widths of Himalayan Hemlock (Tsuga Dumosa). *Atmosphere* 11 (2), 132. doi:10.3390/atmos11020132

Baker, J. C. A., Gloor, M., Spracklen, D. V., Arnold, S. R., Tindall, J. C., Clerici, S. J., et al. (2016). What Drives Interannual Variation in Tree Ring Oxygen Isotopes in the Amazon? *Geophys. Res. Lett.* 43 (22), 11–831. doi:10.1002/2016gl071507

Bao, S., Letu, H., Zhao, J., Lei, Y., Zhao, C., Li, J., et al. (2020). Spatiotemporal Distributions of Cloud Radiative Forcing and Response to Cloud Parameters Over the Mongolian Plateau During 2003-2017. *Int. J. Climatol.* 40 (9), 4082–4101. doi:10.1002/joc.6444

Bhutiyani, M. R., Kale, V. S., and Pawar, N. J. (2008). Changing Streamflow Patterns in the Rivers of Northwestern Himalaya: Implications of Global Warming in the 20th Century. *Curr. Sci.* 95 (5), 618–626.

Bhutiyani, M. R., Kale, V. S., and Pawar, N. J. (2010). Climate Change and the Precipitation Variations in the Northwestern Himalaya: 1866–2006. *Int. J. Climatol.* 30 (4), 535–548. doi:10.1002/joc.1920

Bonekamp, P. N. J., de Kok, R. J., Collier, E., and Immerzeel, W. W. (2019). Contrasting Meteorological Drivers of the Glacier Mass Balance Between the Karakoram and Central Himalaya. *Front. Earth Sci.* 7, 107. doi:10.3389/feart.2019.00107

Bookhagen, B., and Burbank, D. W. (2010). Toward a Complete Himalayan Hydrological Budget: Spatiotemporal Distribution of Snowmelt and Rainfall and Their Impact on River Discharge. *J. Geophys. Res. Earth Surf.* 115 (F3), F03019. doi:10.1029/2009jf001426

Borgaonkar, H. P., Ram, S., and Sikder, A. B. (2009). Assessment of Tree-Ring Analysis of High-Elevation Cedrus Deodara D. Don from Western Himalaya (India) in Relation to Climate and Glacier Fluctuations. *Dendrochronologia* 27 (1), 59–69. doi:10.1016/j.dendro.2008.09.002

Chen, F., Opała-Owczarek, M., Khan, A., Zhang, H., Owczarek, P., Chen, Y., et al. (2021). Late Twentieth Century Rapid Increase in High Asian Seasonal Snow and Glacier-Derived Streamflow Tracked by Tree Rings of the Upper Indus River Basin. *Environ. Res. Lett.* 16 (9), 094055. doi:10.1088/1748-9326/ac1b5c

Collier, E., Mölg, T., Maussion, F., Scherer, D., Mayer, C., and Bush, A. B. G. (2013). High-Resolution Interactive Modelling of the Mountain Glacier-Atmosphere Interface: An Application Over the Karakoram. *Cryosphere* 7 (3), 779–795. doi:10.5194/tc-7-779-2013

Cook, E. R., Palmer, J. G., Ahmed, M., Woodhouse, C. A., Fenwick, P., Zafar, M. U., et al. (2013). Five Centuries of Upper Indus River Flow from Tree Rings. *J. Hydrology* 486, 365–375. doi:10.1016/j.jhydrol.2013.02.004

de Kok, R. J., Kraaijenbrink, P. D. A., Tuinenburg, O. A., Bonekamp, P. N. J., and Immerzeel, W. W. (2020). Towards Understanding the Pattern of Glacier Mass Balances in High Mountain Asia Using Regional Climatic Modelling. *Cryosphere* 14 (9), 3215–3234. doi:10.5194/tc-14-3215-2020

de Kok, R. J., Tuinenburg, O. A., Bonekamp, P. N. J., and Immerzeel, W. W. (2018). Irrigation as a Potential Driver for Anomalous Glacier Behavior in High Mountain Asia. *Geophys. Res. Lett.* 45 (4), 2047–2054. doi:10.1002/2017gl076158

Dirmeyer, P. A., Brubaker, K. L., and DelSole, T. (2009). Import and Export of Atmospheric Water Vapor Between Nations. *J. Hydrology* 365 (1-2), 11–22. doi:10.1016/j.jhydrol.2008.11.016

Duveiller, G., Hooker, J., and Cescatti, A. (2018). The Mark of Vegetation Change on Earth's Surface Energy Balance. *Nat. Commun.* 9 (1), 679. doi:10.1038/s41467-017-02810-8

Fritts, H. C. (1976). *Tree-Rings and Climate*, 567. London: Academic Press.

Fujita, K., and Nuimura, T. (2011). Spatially Heterogeneous Wastage of Himalayan Glaciers. *Proc. Natl. Acad. Sci. U.S.A.* 108 (34), 14011–14014. doi:10.1073/pnas.1106242108

Gaire, N. P., Fan, Z. X., Shah, S. K., Thapa, U. K., and Rokaya, M. B. (2020). *Tree-Ring Record of Winter Temperature from Humla, Karnali, in Central*

Himalaya: A 229 Years-Long Perspective for Recent Warming Trend. Physical Geography: Geografiska Annaler: Series A, 1–20.

Grießinger, J., Bräuning, A., Helle, G., Hochreuther, P., and Schleser, G. (2017). Late Holocene Relative Humidity History on The Southeastern Tibetan Plateau Inferred From A Tree-Ring Δ18o Record: Recent Decrease And Conditions During the Last 1500 Years. *Quat. Int.* 430, 52–59. doi:10.1016/j.quaint.2016.02.011

Harder, P., Pomeroy, J. W., and Helgason, W. (2017). Local-Scale Advection of Sensible and Latent Heat During Snowmelt. *Geophys. Res. Lett.* 44 (19), 9769–9777. doi:10.1002/2017gl074394

Harding, R. J., Blyth, E. M., Tuinenburg, O. A., and Wiltshire, A. (2013). Land Atmosphere Feedbacks and Their Role in the Water Resources of the Ganges Basin. *Sci. Total Environ.* 468-469, S85–S92. doi:10.1016/j.scitotenv.2013.03.016

Harris, I., Jones, P. D., Osborn, T. J., and Lister, D. H. (2014). Updated High-Resolution Grids of Monthly Climatic Observations – The CRU Ts3.10 Dataset. *Int. J. Climatol.* 34 (3), 623–642. doi:10.1002/joc.3711

Haupt, M., Weigl, M., Grabner, M., and Boettger, T. (2011). A 400-Year Reconstruction of July Relative Air Humidity for the Vienna Region (Eastern Austria) Based on Carbon and Oxygen Stable Isotope Ratios in Tree-Ring Latewood Cellulose of Oaks (Quercus Petraea Matt. Liebl.). *Clim. Change* 105, 243–262. doi:10.1007/s10584-010-9862-1

Hochreuther, P., Wernicke, J., Grießinger, J., Mölg, T., Zhu, H., Wang, L., et al. (2016). Influence of the Indian Ocean Dipole on Tree-Ring $\delta^{18}O$ of Monsoonal Southeast Tibet. *Clim. Change* 137 (1-2), 217–230. doi:10.1007/s10584-016-1663-8

Huang, R., Zhu, H., Liang, E., Bräuning, A., Zhong, L., Xu, C., et al. (2022). Contribution of Winter Precipitation to Tree Growth Persists Until the Late Growing Season in the Karakoram of Northern Pakistan. *J. Hydrology* 607, 127513. doi:10.1016/j.jhydrol.2022.127513

Huang, R., Zhu, H., Liang, E., Grießinger, J., Wernicke, J., Yu, W., et al. (2019). Temperature Signals in Tree-Ring Oxygen Isotope Series from the Northern Slope of the Himalaya. *Earth Planet. Sci. Lett.* 506, 455–465. doi:10.1016/j.epsl.2018.11.002

Joswiak, D. R., Yao, T., Wu, G., Tian, L., and Xu, B. (2013). Ice-Core Evidence of Westerly and Monsoon Moisture Contributions in the Central Tibetan Plateau. *J. Glaciol.* 59 (213), 56–66. doi:10.3189/2013jog12j035

Jury, M. W., Mendlik, T., Tani, S., Truhetz, H., Maraun, D., Immerzeel, W. W., et al. (2020). Climate Projections for Glacier Change Modelling over the Himalayas. *Int. J. Climatol.* 40 (3), 1738–1754. doi:10.1002/joc.6298

Kahmen, A., Sachse, D., Arndt, S. K., Tu, K. P., Farrington, H., Vitousek, P. M., et al. (2011). Cellulose (Delta)^{18}o Is an Index Of Leaf-To-Air Vapor Pressure Difference (Vpd) In Tropical Plants. *Proc. Natl. Acad. Sci. U.S.A.* 108 (5), 1981–1986. doi:10.1073/pnas.1018906108

Kapnick, S. B., Delworth, T. L., Ashfaq, M., Malyshev, S., and Milly, P. C. D. (2014). Snowfall Less Sensitive to Warming in Karakoram Than in Himalayas Due to a Unique Seasonal Cycle. *Nat. Geosci.* 7 (11), 834–840. doi:10.1038/ngeo2269

Karki, R., Hasson, S. u., Schickhoff, U., Scholten, T., and Böhner, J. (2017). Rising Precipitation Extremes Across Nepal. *Climate* 5 (1), 4. doi:10.3390/cli5010004

Kaspari, S., Hooke, R. L., Mayewski, P. A., Kang, S., Hou, S., and Qin, D. (2008). Snow Accumulation Rate on Qomolangma (Mount Everest), Himalaya: Synchroneity With Sites Across the Tibetan Plateau on 50-100 Year Timescales. *J. Glaciol.* 54 (185), 343–352. doi:10.3189/002214308784886126

Keys, P. W., Wang-Erlandsson, L., and Gordon, L. J. (2016). Revealing Invisible Water: Moisture Recycling as an Ecosystem Service. *Plos One* 11 (3), e0151993. doi:10.1371/journal.pone.0151993

Khan, A., Chen, F., Ahmed, M., and Zafar, M. U. (2020). Rainfall Reconstruction for the Karakoram Region in Pakistan Since 1540 CE Reveals Out-of-Phase Relationship in Rainfall Between the Southern and Northern Slopes of the Hindukush-Karakorum-Western Himalaya Region. *Int. J. Climatol.* 40 (1), 52–62. doi:10.1002/joc.6193

Kotlia, B. S., Ahmad, S. M., Zhao, J.-X., Raza, W., Collerson, K. D., Joshi, L. M., et al. (2012). Climatic Fluctuations During the LIA and Post-LIA in the Kumaun Lesser Himalaya, India: Evidence from a 400 Y Old Stalagmite Record. *Quat. Int.* 263, 129–138. doi:10.1016/j.quaint.2012.01.025

Kuhn, M. (2015). *Caret: Classification and Regression Training*. Astrophysics Source Code Library. ascl-1505. 2015ascl.soft05003K

Kumar, P., Saharwardi, M. S., Banerjee, A., Azam, M. F., Dubey, A. K., and Murtugudde, R. (2019). Snowfall Variability Dictates Glacier Mass Balance Variability in Himalaya-Karakoram. *Sci. Rep.* 9 (1), 18192–18199. doi:10.1038/s41598-019-54553-9

Lau, W. K. M., Kim, M.-K., Kim, K.-M., and Lee, W.-S. (2010). Enhanced Surface Warming and Accelerated Snow Melt in the Himalayas and Tibetan Plateau Induced by Absorbing Aerosols. *Environ. Res. Lett.* 5 (2), 025204. doi:10.1088/1748-9326/5/2/025204

Lehmann, M. M., Goldsmith, G. R., Mirande-Ney, C., Weigt, R. B., Schönbeck, L., Kahmen, A., et al. (2020). The 18 O-Signal Transfer from Water Vapour to Leaf Water and Assimilates Varies Among Plant Species and Growth Forms. *Plant Cell Environ.* 43 (2), 510–523. doi:10.1111/pce.13682

Lehmann, M. M., Goldsmith, G. R., Schmid, L., Gessler, A., Saurer, M., and Siegwolf, R. T. W. (2018). The Effect of 18 O-Labelled Water Vapour on the Oxygen Isotope Ratio of Water and Assimilates in Plants at High Humidity. *New Phytol.* 217 (1), 105–116. doi:10.1111/nph.14788

Liang, F., Brook, G. A., Kotlia, B. S., Railsback, L. B., Hardt, B., Cheng, H., et al. (2015). Panigarh Cave Stalagmite Evidence of Climate Change in the Indian Central Himalaya Since AD 1256: Monsoon Breaks and Winter Southern Jet Depressions. *Quat. Sci. Rev.* 124, 145–161. doi:10.1016/j.quascirev.2015.07.017

Liu, X., Xu, G., Grießinger, J., An, W., Wang, W., Zeng, X., et al. (2014). A Shift in Cloud Cover Over the Southeastern Tibetan Plateau since 1600: Evidence from Regional Tree-Ring $\delta^{18}O$ and its Linkages to Tropical Oceans. *Quat. Sci. Rev.* 88, 55–68. doi:10.1016/j.quascirev.2014.01.009

Liu, X., Zeng, X., Leavitt, S. W., Wang, W., An, W., Xu, G., et al. (2013). A 400-Year Tree-Ring $\delta^{18}O$ Chronology for the Southeastern Tibetan Plateau: Implications for Inferring Variations of the Regional Hydroclimate. *Glob. Planet. Change* 104, 23–33. doi:10.1016/j.gloplacha.2013.02.005

Managave, S., Shimla, P., Yadav, R. R., Ramesh, R., and Balakrishnan, S. (2020). Contrasting Centennial-Scale Climate Variability in High Mountain Asia Revealed by a Tree-Ring Oxygen Isotope Record from Lahaul-Spiti. *Geophys. Res. Lett.* 47 (4), e2019GL086170. doi:10.1029/2019gl086170

Misra, K. G., Yadav, R. R., and Misra, S. (2015). Satluj River Flow Variations Since AD 1660 Based on Tree-Ring Network of Himalayan Cedar from Western Himalaya, India. *Quat. Int.* 371, 135–143. doi:10.1016/j.quaint.2015.01.015

Molden, D. J., Shrestha, A. B., Immerzeel, W. W., Maharjan, A., Rasul, G., Wester, P., et al. (2022). "The Great Glacier and Snow-Dependent Rivers of Asia and Climate Change: Heading for Troubled Waters," in *Water Security Under Climate Change* (Singapore: Springer), 223–250. doi:10.1007/978-981-16-5493-0_12

Mölg, T., Maussion, F., Yang, W., and Scherer, D. (2012a). The Footprint of Asian Monsoon Dynamics in the Mass and Energy Balance of a Tibetan Glacier. *Cryosphere* 6 (6), 1445–1461. doi:10.5194/tc-6-1445-2012

Mölg, T., Großhauser, M., Hemp, A., Hofer, M., and Marzeion, B. (2012b). Limited Forcing of Glacier Loss Through Land-Cover Change on Kilimanjaro. *Nat. Clim. Change* 2 (4), 254–258. doi:10.1038/nclimate1390

Mölg, T., Maussion, F., Collier, E., Chiang, J. C., and Scherer, D. (2017). Prominent Midlatitude Circulation Signature in High Asia's Surface Climate During Monsoon. *J. Geophys. Res. Atmos.* 122 (23), 12–702. doi:10.1002/2017JD027414

Mölg, T., Maussion, F., and Scherer, D. (2014). Mid-Latitude Westerlies as a Driver of Glacier Variability in Monsoonal High Asia. *Nat. Clim. Change* 4 (1), 68–73. doi:10.1038/nclimate2055

Panthi, S., Fan, Z. X., and Bräuning, A. (2021). Ring Widths of Rhododendron Shrubs Reveal a Persistent Winter Warming in the Central Himalaya. *Dendrochronologia* 65, 125799.

Parida, B. R., Pandey, A. C., and Patel, N. R. (2020). Greening and Browning Trends of Vegetation in India and Their Responses to Climatic and Non-Climatic Drivers. *Climate* 8 (8), 92. doi:10.3390/cli8080092

Pepin, N., Bradley, R. S., Diaz, H. F., Baraër, M., Caceres, E. B., Forsythe, N., et al. (2015). Elevation-Dependent Warming in Mountain Regions of the World. *Nat. Clim. Change* 5 (5), 424–430. doi:10.1038/nclimate2563

Perry, L. B., Matthews, T., Guy, H., Koch, I., Khadka, A., Elmore, A. C., et al. (2020). Precipitation Characteristics and Moisture Source Regions on Mt. Everest in the Khumbu, Nepal. *One Earth* 3 (5), 594–607. doi:10.1016/j.oneear.2020.10.011

Rashid, I., Majeed, U., Aneaus, S., and Pelto, M. (2020). Linking the Recent Glacier Retreat and Depleting Streamflow Patterns with Land System Changes in Kashmir Himalaya, India. *Water* 12 (4), 1168. doi:10.3390/w12041168

Roden, J. S., Bowling, D. R., McDowell, N. G., Bond, B. J., and Ehleringer, J. R. (2005). Carbon and Oxygen Isotope Ratios of Tree Ring Cellulose Along a Precipitation Transect in Oregon, United States. *J. Geophys. Res. Biogeosciences* 110 (G2), G02003. doi:10.1029/2005jg000033

Sakai, A., and Fujita, K. (2017). Contrasting Glacier Responses to Recent Climate Change in High-Mountain Asia. *Sci. Rep.* 7 (1), 13717–13718. doi:10.1038/s41598-017-14256-5

Sano, M., Dimri, A. P., Ramesh, R., Xu, C., Li, Z., and Nakatsuka, T. (2017). Moisture Source Signals Preserved in a 242-Year Tree-Ring $\delta^{18}O$ Chronology in the Western Himalaya. *Glob. Planet. Change* 157, 73–82. doi:10.1016/j.gloplacha.2017.08.009

Sano, M., Ramesh, R., Sheshshayee, M., and Sukumar, R. (2012). Increasing Aridity Over the Past 223 Years in the Nepal Himalaya Inferred from a Tree-Ring $\delta^{18}O$ Chronology. *Holocene* 22 (7), 809–817. doi:10.1177/0959683611430338

Sano, M., Tshering, P., Komori, J., Fujita, K., Xu, C., and Nakatsuka, T. (2013). Precipitation in the Bhutan Himalaya Since 1743 as Reconstructed from Tree Ring Cellulose $\delta^{18}O$. *J. Geophys. Res. Atmos.* 118 (15), 8399–8410. doi:10.1002/jgrd.50664

Shah, S. K., Pandey, U., Mehrotra, N., Wiles, G. C., and Chandra, R. (2019). A Winter Temperature Reconstruction for the Lidder Valley, Kashmir, Northwest Himalaya Based on Tree-Rings of Pinus Wallichiana. *Clim. Dyn.* 53 (7-8), 4059–4075. doi:10.1007/s00382-019-04773-6

Shekhar, M., Bhardwaj, A., Singh, S., Ranhotra, P. S., Bhattacharyya, A., Pal, A. K., et al. (2017). Himalayan Glaciers Experienced Significant Mass Loss During Later Phases of Little Ice Age. *Sci. Rep.* 7 (1), 10305–10314. doi:10.1038/s41598-017-09212-2

Shen, M., Piao, S., Jeong, S.-J., Zhou, L., Zeng, Z., Ciais, P., et al. (2015). Evaporative Cooling Over the Tibetan Plateau Induced by Vegetation Growth. *Proc. Natl. Acad. Sci. U.S.A.* 112 (30), 9299–9304. doi:10.1073/pnas.1504418112

Shrestha, S., Yao, T., and Adhikari, T. R. (2019). Analysis of Rainfall Trends of Two Complex Mountain River Basins on the Southern Slopes of the Central Himalayas. *Atmos. Res.* 215, 99–115. doi:10.1016/j.atmosres.2018.08.027

Sigdel, S. R., Zhang, H., Zhu, H., Muhammad, S., and Liang, E. (2020). Retreating Glacier and Advancing Forest Over the Past 200 Years in the Central Himalayas. *J. Geophys. Res. Biogeosciences* 125 (9), e2020JG005751. doi:10.1029/2020jg005751

Silva, L. C., Sun, G., Zhu-Barker, X., Liang, Q., Wu, N., and Horwath, W. R. (2016). Tree Growth Acceleration and Expansion of Alpine Forests: The Synergistic Effect of Atmospheric and Edaphic Change. *Sci. Adv.* 2 (8), e1501302. doi:10.1126/sciadv.1501302

Singh, J., Park, W. K., and Yadav, R. R. (2006). Tree-Ring-Based Hydrological Records for Western Himalaya, India, Since AD 1560. *Clim. Dyn.* 26 (2-3), 295–303. doi:10.1007/s00382-005-0089-1

Singh, J., Singh, N., Chauhan, P., Yadav, R. R., Bräuning, A., Mayr, C., et al. (2019). Tree-Ring $\delta^{18}O$ Records of Abating June-July Monsoon Rainfall Over the Himalayan Region in the Last 273 Years. *Quat. Int.* 532, 48–56. doi:10.1016/j.quaint.2019.09.030

Singh, J., and Yadav, R. R. (2013). Tree-Ring-Based Seven Century Long Flow Records of Satluj River, Western Himalaya, India. *Quat. Int.* 304, 156–162. doi:10.1016/j.quaint.2013.03.024

Singh, N., Patel, N. R., Bhattacharya, B. K., Soni, P., Parida, B. R., and Parihar, J. S. (2014). Analyzing the Dynamics and Inter-Linkages of Carbon and Water Fluxes in Subtropical Pine (Pinus Roxburghii) Ecosystem. *Agric. For. Meteorology* 197, 206–218. doi:10.1016/j.agrformet.2014.07.004

Singh, N., Shekhar, M., Singh, J., Gupta, A. K., Bräuning, A., Mayr, C., et al. (2021a). Central Himalayan Tree-Ring Isotopes Reveal Increasing Regional Heterogeneity and Enhancement in Ice Mass Loss Since the 1960s. *Cryosphere* 15 (1), 95–112. doi:10.5194/tc-15-95-2021

Singh, N., Singh, J., Gupta, A. K., Bräuning, A., Dimri, A. P., Ramanathan, A. L., et al. (2021b). Climate-Driven Acceleration in Forest Evapotranspiration Fuelling Extreme Rainfall Events in the Himalaya. *Environ. Res. Lett.* 16, 084042. doi:10.1088/1748-9326/ac14ed

Singh, N., Singhal, M., Chhikara, S., Karakoti, I., Chauhan, P., and Dobhal, D. P. (2020). Radiation and Energy Balance Dynamics over a Rapidly Receding Glacier in the Central Himalaya. *Int. J. Climatol.* 40 (1), 400–420. doi:10.1002/joc.6218

Talchabhadel, R., Karki, R., Thapa, B. R., Maharjan, M., and Parajuli, B. (2018). Spatio-Temporal Variability of Extreme Precipitation in Nepal. *Int. J. Climatol.* 38 (11), 4296–4313. doi:10.1002/joc.5669

Thapa, U. K., Shah, S. K., Gaire, N. P., and Bhuju, D. R. (2015). Spring Temperatures in the Far-Western Nepal Himalaya Since AD 1640 Reconstructed from Picea Smithiana Tree-Ring Widths. *Clim. Dyn.* 45 (7-8), 2069–2081. doi:10.1007/s00382-014-2457-1

Treydte, K. S., Schleser, G. H., Helle, G., Frank, D. C., Winiger, M., Haug, G. H., et al. (2006). The Twentieth Century Was the Wettest Period in Northern Pakistan over the Past Millennium. *Nature* 440 (7088), 1179–1182. doi:10.1038/nature04743

Tuinenburg, O. A., Hutjes, R. W. A., and Kabat, P. (2012). The Fate of Evaporated Water from the Ganges Basin. *J. Geophys. Res. Atmos.* 117 (D1), D01107. doi:10.1029/2011jd016221

van Oldenborgh, G. J., and Burgers, G. (2005). Searching for Decadal Variations in ENSO Precipitation Teleconnections. *Geophys. Res. Lett.* 32, L15701. doi:10.1029/2005gl023110

Verma, A., Kumar, A., Gupta, A. K., Tiwari, S. K., Bhambri, R., and Naithani, S. (2018). Hydroclimatic Significance of Stable Isotopes in Precipitation from Glaciers of Garhwal Himalaya, Upper Ganga Basin (UGB), India. *Hydrol. Process.* 32 (12), 1874–1893. doi:10.1002/hyp.13128

Wang, J., Yang, B., and Ljungqvist, F. C. (2020). Moisture and Temperature Covariability Over the Southeastern Tibetan Plateau During the Past Nine Centuries. *J. Clim.* 33 (15), 6583–6598. doi:10.1175/jcli-d-19-0363.1

Wang, R., Liu, S., Shangguan, D., Radić, V., and Zhang, Y. (2019). Spatial Heterogeneity in Glacier Mass-Balance Sensitivity Across High Mountain Asia. *Water* 11 (4), 776. doi:10.3390/w11040776

Watanabe, M., Yanagawa, A., Watanabe, S., Hirabayashi, Y., and Kanae, S. (2019). Quantifying the Range of Future Glacier Mass Change Projections Caused by Differences Among Observed Past-Climate Datasets. *Clim. Dyn.* 53 (3-4), 2425–2435. doi:10.1007/s00382-019-04868-0

Wernicke, J., Hochreuther, P., Grießinger, J., Zhu, H., Wang, L., and Bräuning, A. (2017). Multi-Century Humidity Reconstructions from the Southeastern Tibetan Plateau Inferred from Tree-Ring $\delta^{18}O$. *Glob. Planet. Change* 149, 26–35. doi:10.1016/j.gloplacha.2016.12.013

Wickham, H. (2016). *ggplot2: Elegant Graphics for Data Analysis*. New York, NY: Springer-Verlag. ISBN 978-3-319-24277-4. http://ggplot2.org.

Xu, C., Sano, M., Dimri, A. P., Ramesh, R., Nakatsuka, T., Shi, F., et al. (2018). Decreasing Indian Summer Monsoon on the Northern Indian Sub-Continent During the Last 180 Years: Evidence from Five Tree-Ring Cellulose Oxygen Isotope Chronologies. *Clim. Past* 14 (5), 653–664. doi:10.5194/cp-14-653-2018

Xu, C., Shao, X., An, W., Nakatsuka, T., Zhang, Y., Sano, M., et al. (2017). Negligible Local-Factor Influences on Tree Ring Cellulose $\delta^{18}O$ of Qilian Juniper in the Animaqing Mountains of the Eastern Tibetan Plateau. *Tellus B Chem. Phys. Meteorology* 69 (1), 1391663. doi:10.1080/16000889.2017.1391663

Yadav, J. S., Pratap, B., Gupta, A. K., Dobhal, D. P., Yadav, R. B. S., and Tiwari, S. K. (2019). Spatio-Temporal Variability of Near-Surface Air Temperature in the Dokriani Glacier Catchment (DGC), Central Himalaya. *Theor. Appl. Climatol.* 136 (3-4), 1513–1532. doi:10.1007/s00704-018-2544-z

Yadav, R. R., Gupta, A. K., Kotlia, B. S., Singh, V., Misra, K. G., Yadava, A. K., et al. (2017). Recent Wetting and Glacier Expansion in the Northwest Himalaya and Karakoram. *Sci. Rep.* 7 (1), 6139–6148. doi:10.1038/s41598-017-06388-5

Yadav, R. R., and Bhutiyani, M. R. (2013). Tree-Ring-Based Snowfall Record for Cold Arid Western Himalaya, India Since A.D. 1460. *J. Geophys. Res. Atmos.* 118 (14), 7516–7522. doi:10.1002/jgrd.50583

Yadav, R. R., Park, W. K., Singh, J., and Dubey, B. (2004). Do the Western Himalayas Defy Global Warming? *Geophys. Res. Lett.* 31 (17), L17201. doi:10.1029/2004gl020201

Yao, T., Thompson, L., Yang, W., Yu, W., Gao, Y., Guo, X., et al. (2012). Different Glacier Status with Atmospheric Circulations in Tibetan Plateau and Surroundings. *Nat. Clim. Change* 2 (9), 663–667. doi:10.1038/nclimate1580

Yao, T., Xue, Y., Chen, D., Chen, F., Thompson, L., Cui, P., et al. (2019). Recent Third Pole's Rapid Warming Accompanies Cryospheric Melt and Water Cycle Intensification and Interactions Between Monsoon and Environment: Multidisciplinary Approach with Observations, Modeling, and Analysis. *Bull. Am. Meteorological Soc.* 100 (3), 423–444. doi:10.1175/bams-d-17-0057.1

Zeng, X., Liu, X., Treydte, K., Evans, M. N., Wang, W., An, W., et al. (2017). Climate Signals in Tree-Ring $\delta^{18}O$ and $\delta^{13}C$ from Southeastern Tibet: Insights from Observations and Forward Modelling of Intra- to Interdecadal Variability. *New Phytol.* 216 (4), 1104–1118. doi:10.1111/nph.14750

Zeng, Z., Zhu, Z., Lian, X., Li, L. Z. X., Chen, A., He, X., et al. (2016). Responses of Land Evapotranspiration to Earth's Greening in CMIP5 Earth System Models. *Environ. Res. Lett.* 11 (10), 104006. doi:10.1088/1748-9326/11/10/104006

Zhang, R., Wei, W., Shang, H., Yu, S., Gou, X., Qin, L., et al. (2019). A Tree Ring-Based Record of Annual Mass Balance Changes for the TS. Tuyuksuyskiy Glacier and its Linkages to Climate Change in the Tianshan Mountains. *Quat. Sci. Rev.* 205, 10–21. doi:10.1016/j.quascirev.2018.11.028

Zhao, H., and Moore, G. W. K. (2006). Reduction in Himalayan Snow Accumulation and Weakening of the Trade Winds Over the Pacific Since the 1840s. *Geophys. Res. Lett.* 33 (17), L17709. doi:10.1029/2006gl027339

Conflict of Interest: The authors declare that the research was conducted in the absence of any commercial or financial relationships that could be construed as a potential conflict of interest.

Publisher's Note: All claims expressed in this article are solely those of the authors and do not necessarily represent those of their affiliated organizations, or those of the publisher, the editors and the reviewers. Any product that may be evaluated in this article, or claim that may be made by its manufacturer, is not guaranteed or endorsed by the publisher.

Copyright © 2022 Singh, Shekhar, Parida, Gupta, Sain, Rai, Bräuning, Singh Charkaborty, Sharma, Kamal Tiwari, Chauhan and Montagnani. This is an open-access article distributed under the terms of the Creative Commons Attribution License (CC BY). The use, distribution or reproduction in other forums is permitted, provided the original author(s) and the copyright owner(s) are credited and that the original publication in this journal is cited, in accordance with accepted academic practice. No use, distribution or reproduction is permitted which does not comply with these terms.